Calcineurin determines toxic versus beneficial responses to α-synuclein

Gabriela Caraveo[a,b], Pavan K. Auluck[a,c,1], Luke Whitesell[a], Chee Yeun Chung[a], Valeriya Baru[a,b], Eugene V. Mosharov[d], Xiaohui Yan[e], Manu Ben-Johny[f], Martin Soste[g], Paola Picotti[g], Hanna Kim[e], Kim A. Caldwell[e], Guy A. Caldwell[e], David Sulzer[d,h], David T. Yue[f], and Susan Lindquist[a,b,2]

[a]Whitehead Institute for Biomedical Research, Cambridge, MA 02142; [b]Howard Hughes Medical Institute, Department of Biology, Massachusetts Institute of Technology, Cambridge, MA 02139; [c]Department of Pathology, Massachusetts General Hospital and Harvard Medical School, Boston, MA 02114; Departments of [d]Neurology and [h]Psychiatry, Columbia University Medical Center, New York, NY 10032; [e]Department of Biological Sciences, The University of Alabama, Tuscaloosa, AL 35487; [f]Departments of Biomedical Engineering and Neuroscience, The Johns Hopkins University School of Medicine, Baltimore, MD 21205; and [g]Department of Biology, Institute of Biochemistry, Eidgenossische Technische Hochschule Zurich, Zurich CH-8093, Switzerland

Contributed by Susan Lindquist, July 15, 2014 (sent for review May 7, 2014)

Calcineurin (CN) is a highly conserved Ca^{2+}–calmodulin (CaM)-dependent phosphatase that senses Ca^{2+} concentrations and transduces that information into cellular responses. Ca^{2+} homeostasis is disrupted by α-synuclein (α-syn), a small lipid binding protein whose misfolding and accumulation is a pathological hallmark of several neurodegenerative diseases. We report that α-syn, from yeast to neurons, leads to sustained highly elevated levels of cytoplasmic Ca^{2+}, thereby activating a CaM-CN cascade that engages substrates that result in toxicity. Surprisingly, complete inhibition of CN also results in toxicity. Limiting the availability of CaM shifts CN's spectrum of substrates toward protective pathways. Modulating CN or CN's substrates with highly selective genetic and pharmacological tools (FK506) does the same. FK506 crosses the blood brain barrier, is well tolerated in humans, and is active in neurons and glia. Thus, a tunable response to CN, which has been conserved for a billion years, can be targeted to rebalance the phosphatase's activities from toxic toward beneficial substrates. These findings have immediate therapeutic implications for synucleinopathies.

NFAT | TORC2 | neuroinflammation | Crz1 | Slm2

Cells must tightly regulate Ca^{2+} homeostasis to avoid pathological perturbations and cell death (1). For example, a profound disruption of Ca^{2+} homeostasis is seen in Parkinson disease (PD), the second most common neurodegenerative disorder. Mutations or aberrant expression of α-synuclein (α-syn), a major protein involved in the pathogenesis of PD, can induce Ca^{2+} overload and cell death (2–5). Additional clinical and experimental observations highlight the importance of Ca^{2+} homeostasis in the pathogenesis of PD. Midbrain dopaminergic (DA) neurons that overexpress Ca^{2+}-binding proteins, which buffer intracellular Ca^{2+}, are characteristically spared from degeneration (6). Patients with hypertension who are treated with the L-type Ca^{2+} channel blocker, isradipine, have a lower incidence of PD (7). Moreover, isradipine protects DA neurons incubated with α-syn fibrils and is protective in animal models of toxin-induced PD (8–10).

From yeast to mammals, calcineurin is largely responsible for transducing the signals generated by changes in Ca^{2+} levels (11). Calcineurin (CN) is a calmodulin (CaM)-dependent serine/threonine phosphatase composed of a catalytic subunit (calcineurin A, CNA) and an activating regulatory subunit (calcineurin B, CNB). As intracellular Ca^{2+} levels rise, Ca^{2+} binds to CNB and CaM, another key calcium signaling protein. Together, Ca^{2+}-bound CNB and CaM bind CNA, inducing a conformational change that fully activates the phosphatase (11). Signaling through CN plays critical roles in processes ranging from stress response survival in yeast (12) to mammalian development (13).

Despite the compelling link between Ca^{2+} homeostasis and PD, we know little about the signaling pathways driven by sustained Ca^{2+} elevations and how they might lead to cell death (4, 5). Yeast provide a powerful model system for such investigations, given their genetic tractability and the remarkable conservation of Ca^{2+}-signaling pathways from yeast to humans (14, 15). Moreover, the expression of human α-syn in yeast leads to cellular pathologies directly relevant to neurons and PD, including nitrosative stress (16, 17), defects in vesicle trafficking (18–20), and faulty mitochondrial function (21, 22).

Results

Intracellular Ca^{2+} Is Highly Dependent on α-Syn Dosage. The toxicity of α-syn is extremely dosage sensitive (20, 23). We first asked if the deregulation of Ca^{2+} in yeast shows the same extreme sensitivity to α-syn dosage as does toxicity. We monitored relative cytosolic Ca^{2+} levels in strains expressing different levels of α-syn using the genetically encoded Ca^{2+} sensor, aequorin. Four yeast strains were transformed with a plasmid expressing aequorin (Fig. 1 and Fig. S1*A*): control cells (expressing yellow fluorescent protein, YFP), NoTox (expressing α-syn at low, nontoxic levels), IntTox (expressing α-syn at intermediate, moderately toxic levels), and HiTox (expressing α-syn at a higher, severely toxic level).

In response to α-syn induction, the NoTox strain exhibited a reproducible twofold elevation in cytosolic Ca^{2+}. However, this was transient and Ca^{2+} levels rapidly returned to normal. The IntTox strain exhibited a twofold elevation in cytosolic Ca^{2+} that was stable for 24 h. The HiTox strain, however, reached

Significance

Ca^{2+} homeostasis is indispensable for the well being of all living organisms. Ca^{2+} homeostasis is disrupted by α-synuclein (α-syn), whose misfolding plays a major role in neurodegenerative diseases termed synucleinopathies, such as Parkinson disease. We report that α-syn can induce sustained and highly elevated levels of cytoplasmic Ca^{2+}, thereby activating a calcineurin (CN) cascade that results in toxicity. CN is a highly conserved Ca^{2+}–calmodulin (CaM)-dependent phosphatase critical for sensing Ca^{2+} concentrations and transducing that information into cellular responses. Limiting, but not eliminating, the availability of CaM, CN and/or CN substrates directly with genetic or pharmacological tools shifts the α-syn–induced CN cascade to a protective mode. This has mechanistic implications for CN's activity and provides a therapeutic venue for the treatment of synucleinopathies.

Author contributions: G.C. and S.L. designed research; G.C., P.K.A., V.B., E.V.M., X.Y., M.B.-J., M.S., and H.K. performed research; G.C., C.Y.C., P.P., K.A.C., G.A.C., D.S., and D.T.Y. contributed new reagents/analytic tools; G.C., P.K.A., L.W., P.P., K.A.C., G.A.C., D.S., D.T.Y., and S.L. analyzed data; and G.C. and S.L. wrote the paper.

The authors declare no conflict of interest.

[1]Present address: Translational Pathology Laboratory, Biogen Idec, Inc., Cambridge, MA 02142.

[2]To whom correspondence should be addressed. Email: lindquist@wi.mit.edu.

This article contains supporting information online at www.pnas.org/lookup/suppl/doi:10.1073/pnas.1413201111/-/DCSupplemental.

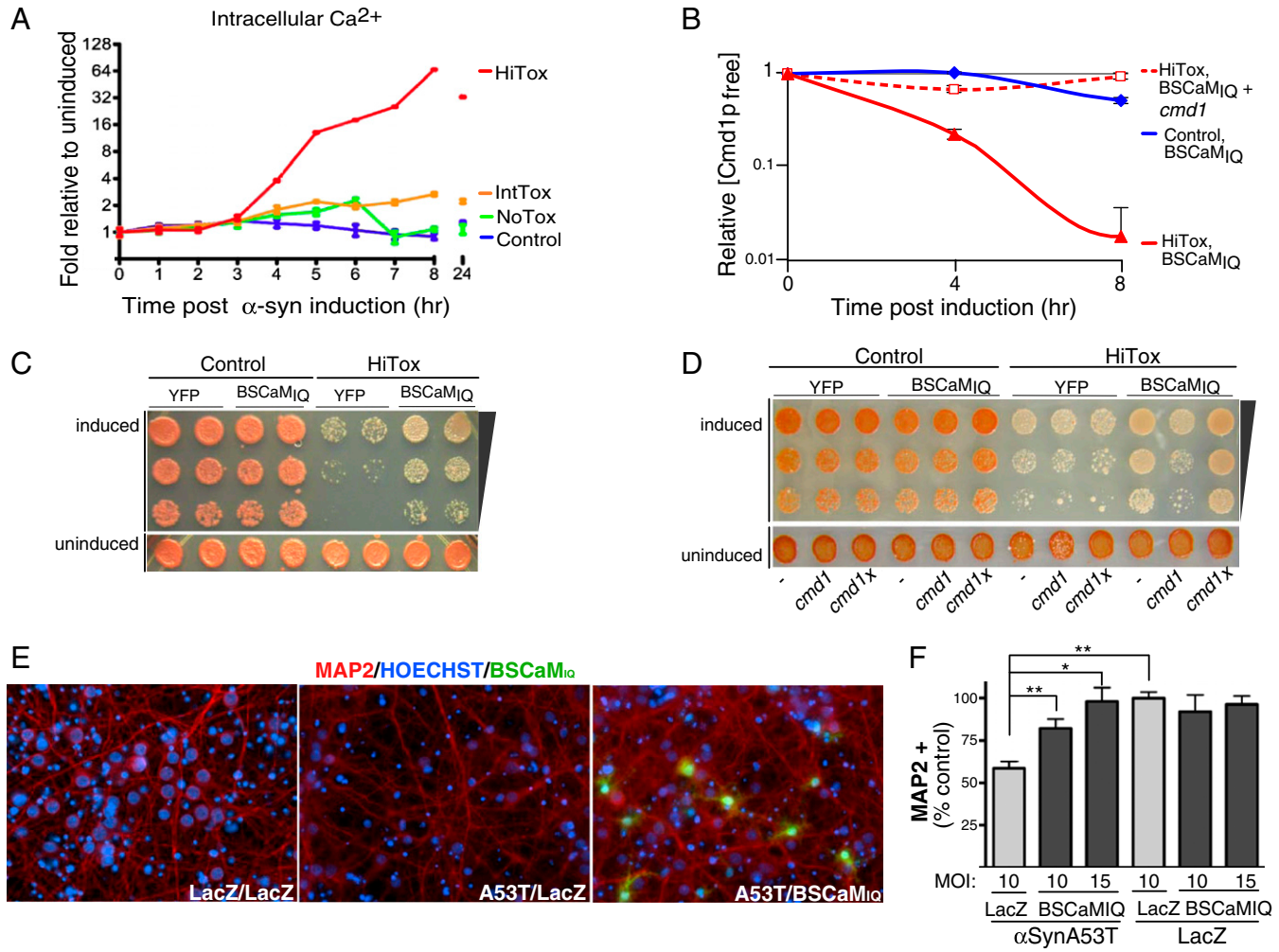

Fig. 1. $BSCaM_{IQ}$, a sensor and a sink for calmodulin, rescues toxicity induced by α-syn by decreasing the total levels of free Ca^{2+}–CaM. (*A*) Strains of control (no α-syn), NoTox (low copy number of α-syn), IntTox (intermediate copy number of α-syn), and HiTox (high copy number of α-syn) were transformed with aequorin, a genetically encoded Ca^{2+} indicator. Cytosolic Ca^{2+} was measured by aequorin luminescence over time after α-syn induction. Cytosolic Ca^{2+} levels are expressed as fold induction relative to control. (*B*) $Cmd1p_{free}$ levels assayed by FRET 0, 4, and 8 h after α-syn induction in the presence of $BSCaM_{IQ}$ in control (blue), HiTox strain (red), and HiTox strain transfected with *cmd1* (red dashed line). $Cmd1p_{free} = K_d$ [(R_{max} − FRET/CFP)/FRET/CFP − R_{min}] (see *Supporting Information*). (*C*) Yeast strains were spotted onto plates containing uninducing media [synthetic defined (SD) −Ura; GPD-$BSCaM_{IQ}$ selective; *Lower*] and replica platted in threefold serial dilutions onto α-syn–inducing plates containing selective media and (SGal −Ura) (*Upper*). YFP is used as control plasmid. (*D*) Yeast strains were spotted onto plates containing uninducing media (SD −Ura, Leu; $BSCaM_{IQ}$ and *cmd1* selective; *Lower*) and replica platted in threefold serial dilutions onto α-syn–inducing plates containing selective media and SGal −Ura, Leu (*Upper*). YFP and empty vector (vec) were used as control plasmids, *cmd1* = yeast calmodulin and $cmd1_X$ = D94A, E105V; unable to bind calcium at the third EF hand. (*E*) $BSCaM_{IQ}$ (green), neuronal (red MAP2 positive), and nuclear (blue, Hoechst) stainings from representative pictures of rat primary neuronal cultures coinfected with either control lentivirus LacZ, LacZ and α-SynA53T, LacZ and α-SynA53T and $BSCaM_{IQ}$, or LacZ and $BSCaM_{IQ}$. (*F*) Percentages of neurons (MAP2 positive) relative to control (LacZ infected) in the conditions described in *B*. *$P < 0.05$, one-way ANOVA, Dunnett's multiple comparison test.

an ∼4-fold elevation in cytosolic Ca^{2+} at 4 h and cytosolic Ca^{2+} continued to climb to an almost 65-fold increase by 8 h (Fig. 1*A*). The rise in Ca^{2+} derived from intracellular stores because it was sensitive to low concentrations of the intracellular calcium chelator 1,2-Bis(2-aminophenoxy)ethane-N,N,N′,N′-tetraacetic acid tetrakis-acetoxymethyl ester, but not to EGTA in the extracellular medium (Fig. S1*B*). Importantly, the extreme elevation in intracellular Ca^{2+} preceded the major onset of cell death in the HiTox strain (Fig. S1*C*). Thus, the release of Ca^{2+} from intracellular stores exhibits strong dependence on the dosage of α-syn and sustained high levels of Ca^{2+} are subsequently associated with extensive cell death.

The Rise in Intracellular Ca^{2+} Is Accompanied by a Decrease in Free Calmodulin. The delay between Ca^{2+} elevation and cell death in the HiTox strain suggested that high Ca^{2+} levels might initiate a cascade of events that are ultimately toxic. Calmodulin (CaM in mammalian cells and Cmd1p in yeast) is a ubiquitous node through which Ca^{2+} activates numerous downstream targets. To determine if CaM plays a direct role in α-syn toxicity, we first expressed a genetically encoded sensor for free CaM (Fig. S2 *A* and *B*). This genetically encoded sensor for free CaM ($BSCaM_{IQ}$) contains a CaM-binding site flanked by CFP and YFP (24, 25). At low Ca^{2+} levels, CaM is largely unbound and is therefore able to bind $BSCaM_{IQ}$. As cytosolic Ca^{2+} rises, CaM engages its targets and binding to $BSCaM_{IQ}$ decreases, resulting in a real-time change in fluorescence resonance energy transfer (FRET) between CFP and YFP. Given that CaM expression is not affected by α-syn in yeast (22), changes in FRET signals from $BSCaM_{IQ}$ provide a quantitative measure of changes in free CaM in our strains.

In the control strain, where cytosolic Ca^{2+} remained low (Fig. 1*A*), free Cmd1p levels remained high and constant (Fig. 1*B*). In the HiTox strain, which experienced a sharp rise in cytosolic Ca^{2+} (Fig. 1*A*), free Cmd1p levels plummeted (Fig. 1*B*). To confirm that the change in FRET with $BSCaM_{IQ}$ was indeed due to a reduction in free Cmd1p, we overexpressed *cmd1*. This restored normal FRET levels in HiTox cells (Fig. 1*B*).

Sequestering Free Calmodulin Ameliorates α-Syn Toxicity in Yeast. The decrease in free CaM caused by α-syn suggests CaM is engaging downstream targets. If this contributes to cell death, the binding of CaM by $BSCaM_{IQ}$ should compete with those targets and reduce toxicity. That is, $BSCaM_{IQ}$ should act not only as a sensor but as a sink for CaM (25) (Fig. S2*C*). To test this, control and HiTox strains expressing $BSCaM_{IQ}$ (or a YFP control) were assayed for growth (Fig. 1*C*). Indeed, expression of $BSCaM_{IQ}$ conferred strong protection to the HiTox strain.

Protection by $BSCaM_{IQ}$ was not due to a trivial effect on α-syn expression (Fig. S2*B*). Nor was it due to a general response to proteotoxic stress because cells expressing proteins associated with other neurodegenerative diseases, polyglutamine expanded huntingtin fragment (Htt) and TDP43, at similarly toxic levels were not rescued by $BSCaM_{IQ}$ (Fig. S2 *D* and *E*).

Expression of $BSCaM_{IQ}$ did not significantly affect Ca^{2+} levels (Fig. S2*F*), suggesting that its protection against cell death was primarily due to the sequestration of Ca^{2+}–CaM. Indeed, the overexpression of wild-type *cmd1* restored toxicity, whereas overexpression of a *cmd1* mutant with impaired Ca^{2+} binding (26) did not (Fig. 1*D* and Fig. S2*G*).

Finally, we tested a completely different CaM sink, the IQ domain from myosin cardiac light chain (CY_{IQ}). This alternative CaM binder also strongly rescued cells from α-syn toxicity (Fig. S2*H*). These findings establish that signaling through Ca^{2+}–CaM-dependent pathways plays an important role in α-syn toxicity in yeast.

Sequestering Free Calmodulin Ameliorates α-Syn Toxicity in Neurons. Next, we asked if Ca^{2+}–CaM was relevant to neuronal α-syn toxicity. We used primary cells derived from rat embryonic cerebral cortices as a model because they are relatively homogenous (more than 80% neurons) and more readily obtained than dopaminergic neurons. Importantly, cortical neurons are strongly affected in patients with PD (27).

Rat embryonic cortical neurons were transduced with a lentivirus that expresses α-syn A53T, a mutation causing an autosomal-dominant form of PD (28) (about 50% infected; Fig. S3*A*). To test the effect of α-syn on Ca^{2+} homeostasis in these neurons, we used the Ca^{2+}-sensitive dye Fluo-4. Infected neurons were visualized with either mKate (control) or an mKate-α-syn fusion regulated by the synapsin promoter. Cells expressing mKate-α-syn had increased basal Ca^{2+} and responded less strongly to KCl-induced depolarization than cells expressing mKate alone (Fig. S3 *B* and *C*). Thus, as previously shown in other primary neuronal models (2–4), overexpression of α-syn perturbs Ca^{2+} homeostasis.

To determine if CaM plays a role in the toxicity of α-syn in neurons, we coinfected A53T-expressing neurons with another lentivirus encoding $BSCaM_{IQ}$ or a control protein, LacZ. Differences in viability were assessed by cellular ATP content as well as by counting the number of cells positive for microtubule-associated protein 2 (MAP2), a neuron-specific marker. $BSCaM_{IQ}$ provided a highly significant, dosage-dependent rescue of α-syn toxicity (Fig. 1 *E* and *F* and Fig. S3*D*).

Calcineurin Activation by Calmodulin Has both Protective and Toxic Roles. A central player in transducing Ca^{2+}–CaM's signals is the highly conserved phosphatase CN (14). To investigate CN's role in α-syn toxicity, we returned to yeast. CN function can be eliminated by deleting the regulatory subunit *cnb1* alone or by the combined deletion of the catalytic subunits *cna1* and *cna2*. As expected (29), neither manipulation affected the growth of the control strain (Fig. 2*A* and Fig. S4*A*). In the HiTox cells,

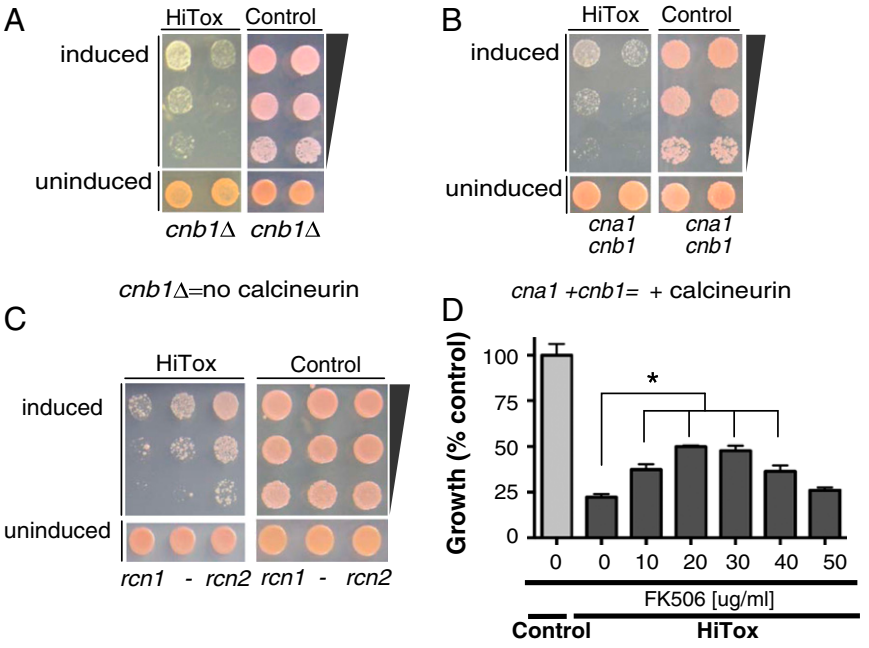

Fig. 2. Calcineurin activation is central to α-syn toxicity in yeast. (*A*) Control and HiTox strains lacking calcineurin (*cnb1*Δ) were spotted onto plates containing uninducing media (SD −His,Trp–α-syn selective, *Lower*) and replica plated in threefold serial dilutions on α-syn–inducing plates containing selective media SGal (*Upper*). (*B*) Control and HiTox yeast strains were spotted onto plates containing uninducing media (SD −Ura, Leu; *cna1*- and *cnb1* selective; *Lower*) and replica plated in threefold serial dilutions onto α-syn–inducing plates containing selective media and SGal (*Upper*). (*C*) Same assay as in *B* except control and HiTox strains was plated onto plates containing uninducing media (SD −Leu; *rcn1*-, or *rcn2* selective, respectively). (*D*) Growth (described as percentage over control) of HiTox cells grown for 48 h over a range of FK506 concentrations. See also Fig. S4*D*.

deleting CN eliminated $BSCaM_{IQ}$ protection (Fig. S4*B*). Because $BSCaM_{IQ}$ acts by titrating CaM, and CaM has many targets, this result suggests that CaM's main effects in response to α-syn toxicity are mediated through the calcineurin pathway.

Surprisingly, however, both deletion and overexpression of CN increased toxicity in the HiTox strain (Fig. 2 *A* and *B*). One explanation for these apparently contradictory results is that an intermediate level of CN activation is protective against α-syn, whereas either too much or too little is detrimental.

As a genetic test of this hypothesis, we used Rcn proteins as negative regulators of CN activity. Rcn1p has a higher affinity for CN than Rcn2p (30). Whereas neither protein affected the control strain, overexpressing *rcn2* (but not *rcn1*) rescued α-syn toxicity (Fig. 2*C*).

As a pharmacological approach, we used FK506. Importantly, FK506 provides a means to continuously vary CN inhibition over a very broad range. FK506 inhibits CN by precisely the same mechanism in yeast and in mammals (29, 31) although higher concentrations of this drug are required in yeast than in mammalian cells (*Materials and Methods*). Consistent with our hypothesis, in the HiTox strain intermediate concentrations of FK506 protected against α-syn toxicity, whereas higher concentrations eliminated this protection (Fig. 2*D*).

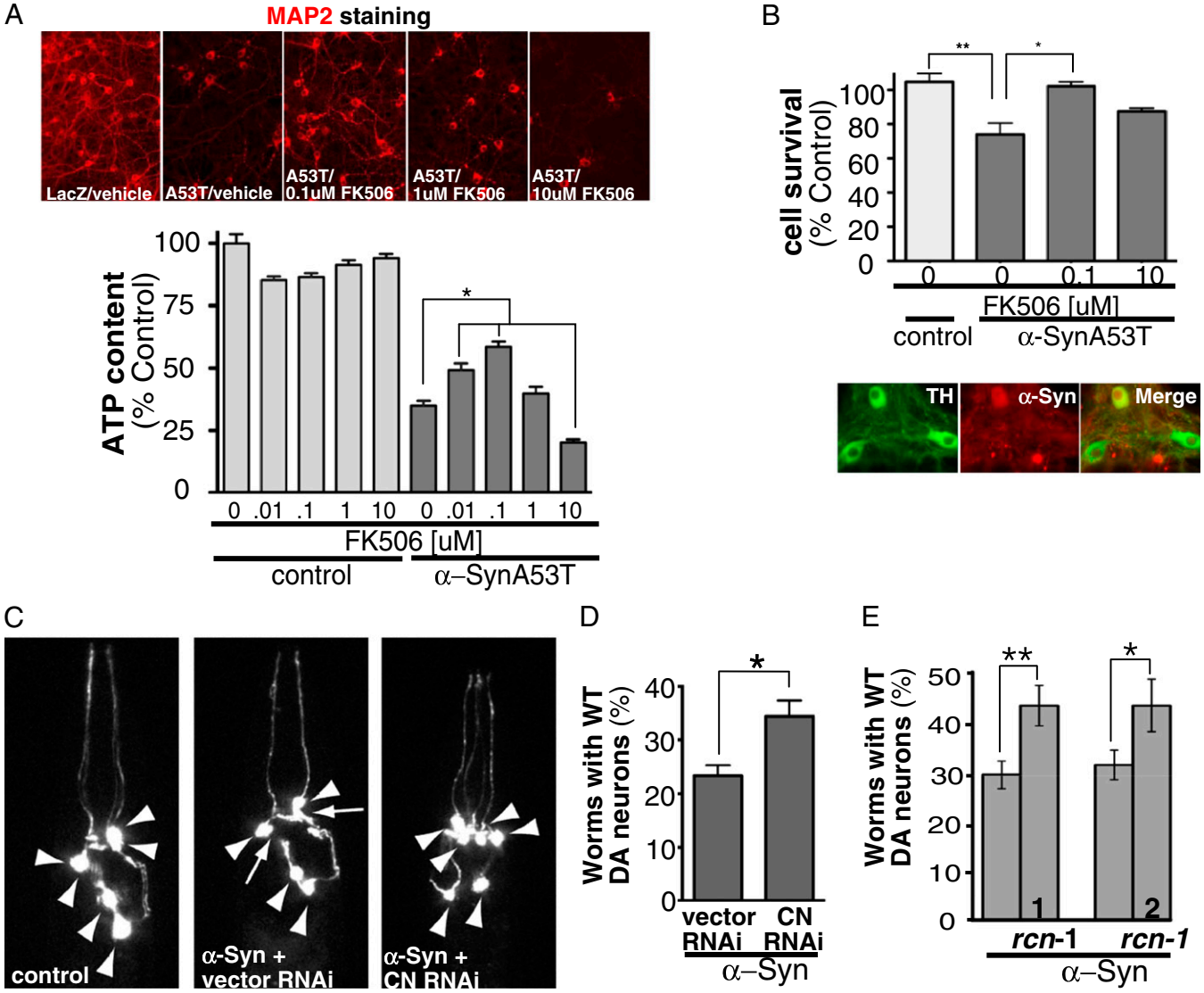

Fig. 3. Partial calcineurin activity is necessary to protect against α-syn toxicity ex vivo and in vivo. (*A*, *Upper*) MAP2 staining from representative pictures of rat primary neuronal cultures coinfected with a lentivirus carrying LacZ as control and/or α-synA53T treated with various doses of FK506 for 14 d. (*Lower*) Rat cortical neurons infected with α-synA53T and/or LacZ as control treated with vehicle and/or increasing concentrations of FK506 for 14 d and assayed for viability for ATP content. $*P < 0.05$, one-way ANOVA, Dunnett's multiple comparison test. Each data point was normalized against control LacZ at the same FK506 dose. (*B*, *Upper*) Dopaminergic neurons from mice infected with α-synA53T and/or mKate as control treated with vehicle and/or distinct concentrations of FK506. Cell survival was measured by counting TH positive neurons after 14 d of α-synA53T infection and drug treatment. $*P < 0.05$, one-way ANOVA, Dunnett's multiple comparison test. (*Lower*) Representative pictures of infection efficiency of mKate α-syn in TH positive neurons. (*C*) Representative images of *C. elegans* dopaminergic neurons in worms expressing GFP alone (*Left*, all six anterior neurons are intact) and in α-syn–expressing worms treated with RNAi control (only four anterior DA neurons remain) or with RNAi for calcineurin (CN) (*Right*). Arrowheads show intact dopaminergic neuron cell bodies and arrows represent areas where dopaminergic neurons are absent. (*D*) The population of worms with WT (wild type) numbers of neurons remaining after treatment with RNAi for calcineurin (CN) or empty vector RNAi (control) in α-syn–expressing worms. For each experiment, three independent experiments were performed, with 30 worms per trial. $*P < 0.05$ (Student *t* test). See also Fig. S5*C*. (*E*) Same assay as in *D* except with worms overexpressing *rcn-1*. Bars 1 and 2 represent independent transgenic lines. $*P < 0.005$, $**P < 0.0005$ (Student *t* test). See also Fig. S5*B*.

Importantly, rescue by intermediate concentrations of FK506 in the HiTox strain was not due to a trivial effect on α-syn expression (Fig. S4*C*). Furthermore, the lack of rescue at high concentrations was not due to off-target toxicity, because FK506 had no effect on control cells even at the highest concentrations used (Fig. S4*D*). Moreover, FK506 effects were specific to the HiTox strain where CN activity is high: the compound had no effect on the less toxic IntTox strain, which has much lower levels of cytosolic Ca^{2+} (Fig. 1*A* and Fig. S4*E*). We further confirmed FK506 effects on CN activity using $BSCaM_{IQ}$, which sequesters CaM and reduces CN activation. The effects of FK506 should be greatly reduced in HiTox cells carrying $BSCaM_{IQ}$, and indeed they were (Fig. S4*F*).

Thus, both genetic and pharmacologic experiments in yeast confirm that an intermediate level of CN inhibition balances the protective versus toxic effects of Ca^{2+}–CaM/CN in response to α-syn.

Decreasing Calcineurin Activity Protects Against α-Syn Toxicity in Neuronal Models. Next, we asked if modulating CN activities could balance toxic versus protective responses to α-syn in primary rat cortical neurons. At all concentrations, FK506 had only a minor effect on the viability of neurons expressing the control protein LacZ (Fig. 3*A*). Intermediate concentrations of FK506 rescued neurons from the toxic effect of α-syn expression. (Note, in keeping with the fact that neurons have many more mechanisms for buffering calcium than yeast cells do, the concentration range for rescue was much broader in neurons than in yeast, spanning a 100-fold range.) Higher concentrations of FK506 were not protective and, in fact, increased toxicity (Fig. 3*A*).

We next asked if FK506 was protective in dopaminergic neurons, the cell type most classically implicated in Parkinson disease. We used primary cultures containing 30–40% dopaminergic neurons assessed by tyrosine hydroxylase (TH) positivity. To allow unambiguous identification, we infected neurons with an adeno-associated virus encoding human $\alpha\text{-syn}^{A53T}$ tagged with mKate or with mKate alone (Fig. S5*A*). Fourteen days after infection, ∼30% of the dopaminergic neurons expressing α-syn had died. Intermediate levels of FK506 rescued cells from α-syn toxicity, whereas the protective effects of the drug disappeared at higher doses (Fig. 3*B*).

To begin moving into multicellular organisms, we took advantage of a previously established nematode model of α-syn toxicity (32). In these worms, GFP and α-syn are both under the transcriptional control of the dopaminergic neuron-specific *dat-1* promoter. Wild-type (WT) worms invariably have six dopaminergic neurons. As previously reported (18), expression of α-syn caused an age- and dose-dependent degeneration of dopaminergic neurons (Fig. 3*C*). We down-regulated CN activity in this model using two methods: direct knockdown of CN with RNAi and overexpression of its negative regulator, *rcn-1*.

To allow RNAi targeting of CN in DA neurons, we expressed the dsRNA transporter SID-1 in these cells using the *dat-1* promoter (33). Knockdown of the catalytic subunit of CN, *tax-6*, had no effect on the dopaminergic neurons of control worms

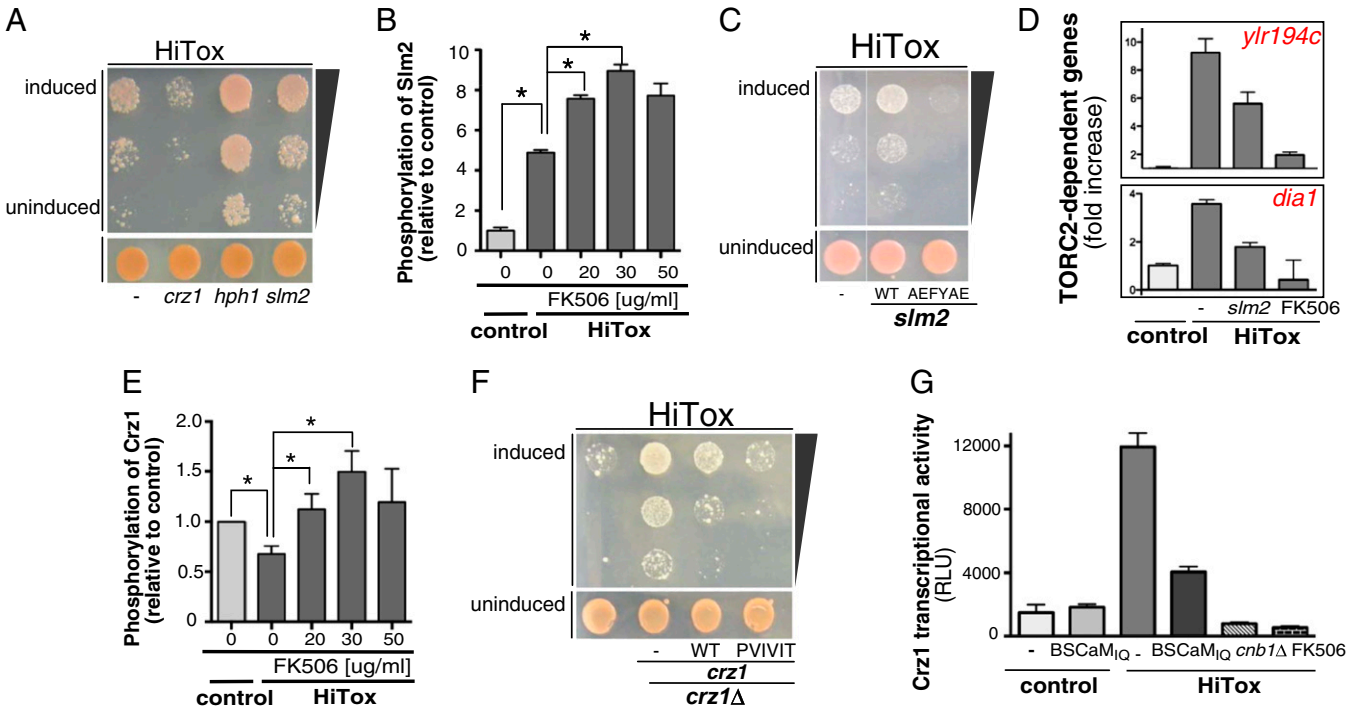

Fig. 4. Calcineurin can activate protective and toxic substrates in yeast. (*A*) The HiTox yeast strain was spotted onto plates containing uninducing media (SD −Leu; vector, *hph1*, *slm2*, or *crz1* selective; *Lower*) and replica plated in threefold serial dilutions onto α-syn–inducing plates containing selective media and SGal −Leu (*Upper*). (*B*) Peak intensity of phosphopeptide ENVD(phospho)SPR from Slm2p relative to control using SRM-mass spectrometry after phosphopeptide enrichment as described (66). Error bars reflect biological and technical variability. *$P < 0.05$ (Student *t* test). (*C*) Similar spotting assays as described in *A* but onto plates containing uninducing media [SD −Leu; *slm2*, *slm2-AEFYAE* (unable to bind calcineurin) selective; *Lower*] and replica plated in threefold serial dilutions onto α-syn–inducing plates containing selective media and SGal −Leu (*Upper*). (*D*) Real-time PCR for the TORC2-dependent genes *ylr194c* and *dia1* in control and HiTox yeast strains in the presence of *slm2* or a low dose of FK506 (25 μg/mL). (*E*) Peak intensity of phosphopeptide MDSANS(phospho)SEKISK from Crz1p relative to control using SRM-mass spectrometry after phosphopeptide enrichment as described (66). Error bars reflect technical variability. *$P < 0.05$ (Student *t* test). (*F*) The HiTox yeast strain was spotted onto plates containing uninducing media [SD −Leu; vector, *crz1*, PVIVIT-*crz1* (high affinity to calcineurin) selective; *Lower*] and replica plated in threefold serial dilutions onto α-syn–inducing plates containing selective media and SGal −Leu (*Upper*) in the presence and absence of *crz1* (*crz1*Δ). (*G*) β-Glactosidase luminescent assay for control and HiTox strains harboring a reporter for crz1p-dependent transcriptional activity in the presence and absence of 25 μg/mL FK506, calcineurin (*cnb1*Δ), and/or $BSCaM_{IQ}$.

(Fig. S5*C*). However, in α-syn–expressing worms, reducing the expression of CN by knockdown protected against toxicity (Fig. 3 *C* and *D*).

Nematodes have only one known negative regulator of CN, *rcn-1* (34). Several independent transgenic lines were established with different levels of *rcn-1* expression. In two transgenic lines, we found that moderate *rcn-1* expression was nontoxic (Fig. S5*B*) and also protected dopaminergic neurons against α-syn toxicity (Fig. 3*E*). Thus, establishing a biological mechanism conserved from single cells (yeast and primary mammalian neurons) to whole worms, chemical and genetic approaches, demonstrate that moderating CN activity is protective against α-syn toxicity.

Protective and Toxic Downstream Substrates of Calcineurin. Our finding that an intermediate level of CN activity is protective against α-syn suggests that some CN downstream targets provide protection, whereas others enhance toxicity. To investigate, we returned to yeast, focusing on three of CN's best characterized substrates: Hph1p, Slm2p, and Crz1p. Remarkably, the processes regulated by all of these proteins are disturbed by α-syn in yeast and in neurons. Hph1p facilitates the posttranslational translocation of proteins, especially those involved in vacuolar ion homeostasis and vesicular trafficking (35). Slm2p acts via the target of rapamycin complex 2 (TORC2) to support cytoskeletal organization and lipid homeostasis (20, 36–38). Crz1p is a transcription factor activated by calcineurin in response to various stresses (39). Importantly, overexpression of these genes under nonstress conditions had no effect on control cells (Fig. S6*A*).

Overexpressing *hph1* or *slm2* rescued α-syn toxicity in the HiTox strain (Fig. 4*A*). Overexpressing *crz1*, however, slightly enhanced toxicity. To better characterize this enhancement of toxicity, we overexpressed *crz1* in the HiTox strain in the presence of $BSCaM_{IQ}$. Overexpression of *crz1* completely abrogated the protective effects of $BSCaM_{IQ}$, confirming the role of *crz1* in enhancing α-syn toxicity and validating the effect of $BSCaM_{IQ}$ on the CN pathway (Fig. S6*B*). Thus, Hph1p and Slm2p drive protective pathways in response to α-syn, whereas Crz1p drives detrimental ones.

We focused further on the protective substrate Slm2p and the toxic substrate Crz1p, because Slm2p and Crz1p pathways are

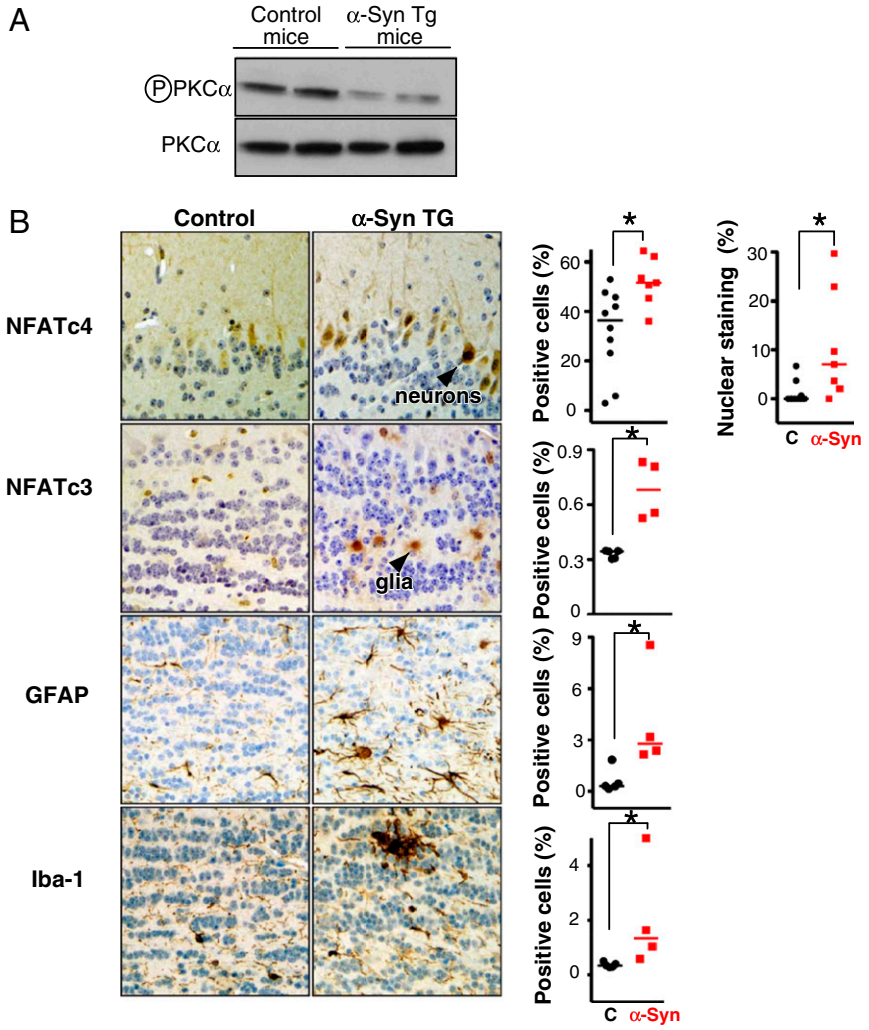

Fig. 5. Calcineurin substrates in α-syn transgenic mice. (*A*) Western blot for phosphoserine 657, PKCα from brain lysates of 12-mo-old α-syn transgenic mice. PKCα serves as loading control. (*B*) Immunohistochemistry for NFATc4 in neurons from the mitral cell layer in the olfactory bulb of 13-mo-old α-syn transgenic mice and control (C) mice (*Upper*). Immunohistochemistry for NFATc3 in glia from the internal plexiform layer in the olfactory bulb of 13-mo-old α-syn transgenic. Immunohistochemistry for glial fibrillary acid protein (GFAP) for normal and reactive astrocytes in the internal plexiform layer of the olfactory bulb. Similarly, immunostaining for Iba-1 from normal and activated microglia in the nodules of the internal plexiform layer of the olfactory bulb of α-syn transgenic mice. Error bars reflect variability between two sections analyzed from a total of five animals in each group. *$P < 0.05$ (Student *t* test).

conserved from yeast to humans. Because CN is a phosphatase, we began by investigating the effect of α-syn on the phosphorylation status of Slm2p and Crz1p using selected reaction monitoring (SRM)-based mass spectrometry (MS) (40). This technique avoids the use of artificial protein tags, which can interfere with protein function, and more importantly, gives information about the nature of the phosphorylation sites in a highly specific and quantitative manner.

α-Syn expression increased Slm2p phosphorylation. Protective doses of FK506 further increased phosphorylation, whereas toxic doses blunted it (Fig. 4*B*). Although the role(s) of phosphorylation in regulating Slm2p activity is not clear, this result is consistant with an interaction between CN and Slm2p driving a protective response against α-syn toxicity. To test this, point mutations in Slm2p that selectively abrogate its interaction with CN (41) eliminated protection against α-syn toxicity, although having no effect on control strains (Fig. 4*C* and Fig. S6*C*).

Slm2p acts upon the TORC2 signaling pathway (38). To see whether this pathway is also affected by α-syn, we assayed the expression of two yeast genes that are classically up-regulated when TORC2 is inhibited (42). *ylr194c* and *dia1* were both up-regulated in response to α-syn expression, indicating that α-syn does indeed inhibit the TORC2 pathway (Fig. 4*D*). As predicted from their effects on CN, overexpression of *slm2* or moderate concentrations of FK506 both decreased expression of *ylr194c* and *dia1*, indicating a restoration of TORC2 function (Fig. 4*D*).

Activation of the transcription factor Crz1p is normally protective for yeast cells under stress (39). However, our results suggest that Crz1p drives a toxic response to α-syn. Phosphorylation of Crz1p inhibits its transcriptional activity. Using SRM to monitor Crz1p phosphorylation, we found that it was reduced in response to α-syn, whereas protective and toxic doses of FK506 increased it (Fig. 4*E*). A mutant of Crz1p with increased affinity for CN (43) had no effect on control cells but increased toxicity in cells expressing α-syn (Fig. 4*F* and Fig. S6*D*). This high-affinity allele of *crz1* also reduced the protective effect of $BSCaM_{IQ}$, confirming that CaM's role in α-syn toxicity is mediated through the CN pathway (Fig. S6*E*). Further, deleting *crz1* strongly rescued growth in HiTox cells (Fig. 4*F* and Fig. S6*D*).

If Crz1 activation is indeed driving a toxic transcriptional response to α-syn, Crz1p's transcriptional activity should be up-regulated in the HiTox strain. Moreover, if this activity is connected to the Ca^{2+}–CaM/CN pathway cascade, it should be down-regulated by $BSCaM_{IQ}$, by protective concentrations of FK506 or by deletion of CN. Using a β-galactosidase reporter for Crz1p transcriptional activity (44), each of these predictions was fulfilled (Fig. 4*G*). Thus, α-syn activates a toxic Crz1p-regulated response to Ca^{2+} in yeast. Moderate inhibition of CN activity prevents activation of this toxic pathway while still allowing protective responses mediated through substrates such as Slm2p to remain intact.

Downstream Consequences of Calcineurin Activation by α-Syn in Mice. To determine whether the effects of α-syn demonstrated in yeast are conserved in the central nervous system of mammals, we turned to an α-syn transgenic mouse model where α-syn is overexpressed in various regions of the brain, including areas affected in PD such as the olfactory bulb and cortex (45, 46). As they age, these mice display phenotypes reminiscent of PD, including neuroinflammation (increased numbers of astrocytes and microglia), as well as neuronal pathology. Calcineurin is highly expressed in both glia and neurons and, hence, could potentially contribute to protective or toxic responses in both.

First, we probed the status of the TORC2 pathway (activation was protective in yeast). In the brains of 12-mo-old mice, we monitored protein kinase C alpha (PKCα) phosphorylation at serine 657, a canonical downstream substrate of TORC2. PKCα phosphorylation was reduced in brain extracts from α-syn–overexpressing mice compared with controls (Fig. 5*A*). Thus, the inhibition of PKCα correlates with inhibition of the TORC2 pathway in mammalian brain in response to α-syn.

Although no direct homolog of *crz1* exists in mammalian cells, nuclear factor of activated T cells (NFAT) is broadly accepted as its functional analog (41). Similar to Crz1p, calcineurin dephosphorylates various isoforms of NFAT, leading to their nuclear translocation. We monitored two isoforms, NFATc4 and NFATc3, which we found to be prominent in neurons and glia, respectively. In agreement with our yeast results, the neurons from the olfactory bulbs of the α-syn transgenic mice displayed increased nuclear neuronal localization of NFATc4, consistent with its activation (Fig. 5*B*). NFATc3 staining intensity and nuclear localization was increased in glia (Fig. 5*B*), indicating that it, too, was activated. Thus, a calcineurin-mediated response to α-syn was also conserved in the mammalian brain, in both neurons and glia.

NFAT Is Activated in Human Synucleinopathies. Finally, we examined NFAT activation in fixed postmortem tissue from humans diagnosed with PD or with a more aggressive synucleinopathy, dementia with Lewy bodies (DLB). We could not detect NFATc3; however, staining of NFATc4 was highly reproducible

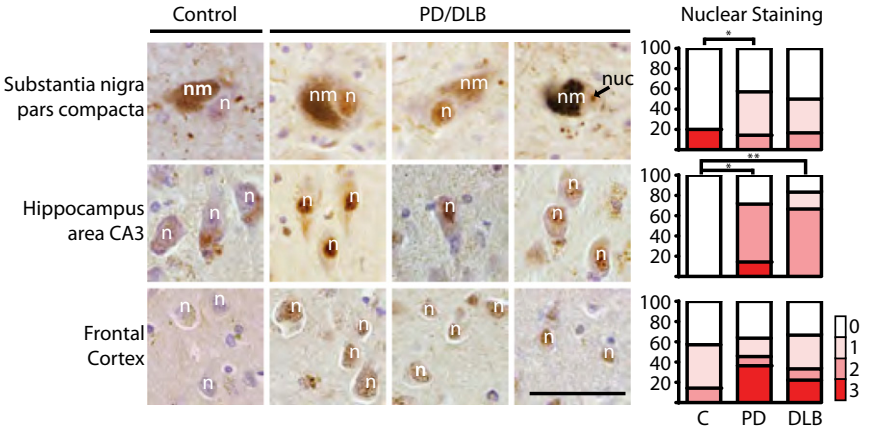

Fig. 6. NFATc4 nuclear expression is increased in cases of PD and DLB. Immunohistochemistry for NFATc4 staining in neurons from the substantia nigra pars compacta, hippocampus area CA3, and layers 5 and 6 of the frontal cortex in human PD and DLB cases. An average of two sections from five control (C) and eight diseased cases were analyzed. Nuclear staining was scored by a neuropathologist. Scoring: 0, no nuclear staining; 1, scattered positive nuclei; 2, positive nuclear <30% of neurons; 3, positive nuclei focally >30% of neurons. n, neuronal nucleus; nm, neuromelanin; nuc, nucleolus. (Scale bar, 50 μm.) *$P < 0.05$ (Student *t* test).

and specific, as it was competed with a peptide that was used to raise the antibody (Fig. S7). Four of the five brains we analyzed from nondiseased controls exhibited cytoplasmic but no nuclear staining for NFATc4. In contrast, NFATc4 immunoreactivity was localized to nuclei in most of the eight cases of PD and DLB consistent with its activation (Fig. 6).

The nuclear staining for NFATc4 in the diseased brains was evident across several different brain regions including the substantia nigra pars compacta (SNc), hippocampus, and frontal cortex, among others. In the frontal and cingulate cortices, nuclear NFATc4 staining was most prominent in the pyramidal neurons in layers 5 and 6. In DLB, these cortical layers bear the greatest burden of α-syn pathology (27). In the hippocampus, which is also critically involved in PD pathology (47), areas CA3 and CA4 stained more strongly than CA1 or CA2 or the subiculum. These results support an association between NFATc4 nuclear localization/activation and α-syn toxicity in human disease.

Discussion

We demonstrate that increasing levels of α-syn expression proportionally increase cytosolic Ca^{2+} concentrations, paralleling the extremely strong dosage dependence of α-syn toxicity previously described in our yeast models (18, 20) and in humans (23, 48). Sustained high cytosolic Ca^{2+} levels drive a Ca^{2+}–CaM–calcineurin cascade that activates a toxic program regulated by the transcription factor Crz1p in yeast and NFAT in mammalian cells. However, calcineurin activation also triggers protective responses against α-syn involving TORC2. The balance between these responses and presumably other unidentified calcineurin substrates is critical in determining the ultimate outcome of activating the Ca^{2+}–CaM–calcineurin pathway in response to α-syn (Fig. S8). Importantly, this multifaceted calcineurin-mediated response to α-syn, although first uncovered in yeast, is conserved in nematodes as well as mammalian neurons, glia, and brains, as, indeed, are the protective effects of moderate concentrations of FK506.

How does α-syn lead to increased cytosolic Ca^{2+}? Our data clearly indicate that it is released from intracellular stores. Given the lipid-binding properties of α-syn, the protein might perturb Ca^{2+} homeostasis directly (through damage to the membrane or membrane channels) or indirectly [as a consequence of the profound block in endoplasmic reticulum (ER) to Golgi trafficking]. How might increased cytosolic Ca^{2+} determine calcineurin's switch between protective and toxic substrates in a concentration-dependent manner? Differences in the sequence and accessibility of substrate docking sites, expression levels, and the number of dephosphorylations required to alter a substrate's activity are all likely involved. These, in turn, will interface with differences in the degree of calcineurin activation, determined by cellular levels of CaM and Ca^{2+} in different compartments within the cell. Given the complexity of this problem, many strategies, including the use of genetically tractable organisms such as yeast, will be required to achieve a full understanding.

Because inhibition of calcineurin activity is routinely exploited clinically through the use of FK506 (tacrolimus) as an immunosuppressant, we now suggest that the repurposing of FK506, a compound that readily traverses the blood brain barrier merits investigation in the management of PD. Because it persists in the central nervous system long after systemic effects have resolved (49), intermittent dosing with this already FDA-approved drug could avoid systemic immunosuppression, while still providing a readily implemented, disease-modifying treatment strategy that targets a fundamental mechanism in the pathogenesis of α-synucleinopathies.

Indeed, FK506 was previously shown to have neuroprotective properties in mammalian PD models (50–53). Because FK506 impairs calcineurin function by locking it into a complex with FKBP12, FK506's neuroprotective effects were thought to be mediated through FKBP12. Compounds that target FKBP12, without affecting calcineurin function, prevented neurodegeneration in specific animal models (54, 55) but failed to show reversal of PD motor symptoms in humans (56). Although we have yet to address any potential contributions of FKBP12 to the protective effects of FK506 that we have seen, our findings clearly establish the importance of reducing calcineurin activity to achieve neuroprotection.

Finally, our findings help explain why in PD, DA neurons in the SNc are particularly sensitive to α-syn–related dysfunction. Adult neurons in the SNc rely on voltage-dependent Ca^{2+} channels. These channels are regulated by CaM binding (57, 58) and drive autonomous pacemaking, which leads to relatively sustained elevations in cytosolic Ca^{2+} (9, 59). Intriguingly, CaM can be cross-linked to α-syn (60, 61), suggesting that α-syn could be locally sequestering CaM to further increase cytosolic Ca^{2+} flux through these channels. Moreover, SNc neurons have higher cytosolic dopamine levels than the less susceptible ventral tegmentum DA neurons (62). This neurotransmitter renders SNc neurons more susceptible to cell death and has also been linked to increased intracellular Ca^{2+} levels (62). The enhanced sensitivity of the SNc DA neurons to Ca^{2+} stress would exacerbate the defects in vesicle trafficking (18, 63, 64), mitochondrial dysfunction (21, 22), nitrosative stress (16, 17), and metal ion homeostasis (65) caused by α-syn. The combination is poised to create the "perfect storm" that devastates the SNc of patients with PD.

Materials and Methods

Primary Cells and Strains. Yeast strains containing α-syn were generated and induced as previously described (18). Rat cortical and mouse dopaminergic neurons were infected with a lentivirus carrying α-syn as described in *SI Materials and Methods*. In vivo models for α-syn in *Caenorhabditis elegans* and mice where generated as described (32, 46). Human samples from PD and DLB patients were obtained through the Massachusetts Alzheimer Disease Research Center as described in *SI Materials and Methods*.

Imaging Techniques. Ca^{2+} imaging was performed using aequorin (in yeast) and Fluo-4 (in neurons). CaM measurements were performed using FRET. MAP2 and TH staining in neurons were performed by immunofluorescence. NFAT staining in mice and human samples were performed by immunohistochemistry. Detailed description of all imaging techniques can be found in *SI Materials and Methods*.

Viability Assays. For neurons we used ATP and MAP2 positive staining, whereas for yeast cells, spotting assays, growth curves using OD_{600}, and propidium idodine incorporation by cell cytometry were performed as viability assays. Detailed description of all viability techniques can be found in *SI Materials and Methods*.

Biochemistry Assays. To monitor phosphorylation of substrates selected reaction monitoring assays was performed. To monitor Crz1p activity in yeast we used the Crz1-dependent reporter element-luciferase reporter (44). Detailed description of these techniques can be found in *SI Materials and Methods*.

Molecular Biology. RCN-1 overexpression and quantitation *C. elegans* was performed as described (34). RNA interference (RNAi) in *C. elegans* was performed as described (33). CaM mutants were performed by QuikChange XL site-directed mutagenesis as described in *SI Materials and Methods*.

ACKNOWLEDGMENTS. Special thanks to Y. Schmitz, A. Mungenast, J. Heitman, M. Cyert, D. Petranovic, and members of the S.L. laboratory for discussions and/or critical reading of the manuscript. This work was supported by the Picower Foundation, the JPB Foundation, a Howard Hughes Medical Institute (HHMI) Collaborative Innovation Award, and the Eleanor Schwartz Charitable Foundation. C.Y.C. is supported by National Institutes of Health (NIH) Grant K01 AG038546, P.K.A., by a Beeson Career Development Award in Aging (NIH Grant K08 AG042774). E.V.M. and D.S. are supported by the JPB and Parkinson's Disease Foundation and the Udall Center of Excellence. E.V.M. is also supported by National Institute of Neurological Disorders and Stroke Grant R01 NS075222. S.L. is an HHMI Investigator.

1. Wojda U, Salinska E, Kuznicki J (2008) Calcium ions in neuronal degeneration. *IUBMB Life* 60(9):575–590.
2. Adamczyk A, Strosznajder JB (2006) Alpha-synuclein potentiates Ca2+ influx through voltage-dependent Ca2+ channels. *Neuroreport* 17(18):1883–1886.
3. Danzer KM, et al. (2007) Different species of alpha-synuclein oligomers induce calcium influx and seeding. *J Neurosci* 27(34):9220–9232.
4. Martin ZS, et al. (2012) α-Synuclein oligomers oppose long-term potentiation and impair memory through a calcineurin-dependent mechanism: Relevance to human synucleopathic diseases. *J Neurochem* 120(3):440–452.
5. Buttner S, et al. (2012) The Ca2+/Mn2+ ion-pump PMR1 links elevation of cytosolic Ca2+ levels to alpha-synuclein toxicity in Parkinson's disease models. *Cell Death Differ* 20(3):465–77.
6. Hurley MJ, Brandon B, Gentleman SM, Dexter DT (2013) Parkinson's disease is associated with altered expression of CaV1 channels and calcium-binding proteins. *Brain* 136(Pt 7):2077–2097.
7. Pasternak B, et al. (2012) Use of calcium channel blockers and Parkinson's disease. *Am J Epidemiol* 175(7):627–635.
8. Dryanovski DI, et al. (2013) Calcium entry and α-synuclein inclusions elevate dendritic mitochondrial oxidant stress in dopaminergic neurons. *J Neurosci* 33(24):10154–10164.
9. Chan CS, et al. (2007) 'Rejuvenation' protects neurons in mouse models of Parkinson's disease. *Nature* 447(7148):1081–1086.
10. Kupsch A, et al. (1996) 1-Methyl-4-phenyl-1,2,3,6-tetrahydropyridine-induced neurotoxicity in non-human primates is antagonized by pretreatment with nimodipine at the nigral, but not at the striatal level. *Brain Res* 741(1-2):185–196.
11. Li H, Rao A, Hogan PG (2011) Interaction of calcineurin with substrates and targeting proteins. *Trends Cell Biol* 21(2):91–103.
12. Bonilla M, Cunningham KW (2002) Calcium release and influx in yeast: TRPC and VGCC rule another kingdom. *Sci STKE* 2002(127):pe17.
13. Graef IA, Chen F, Crabtree GR (2001) NFAT signaling in vertebrate development. *Curr Opin Genet Dev* 11(5):505–512.
14. Rusnak F, Mertz P (2000) Calcineurin: Form and function. *Physiol Rev* 80(4):1483–1521.
15. Auluck PK, Caraveo G, Lindquist S (2010) α-Synuclein: Membrane interactions and toxicity in Parkinson's disease. *Annu Rev Cell Dev Biol* 26:211–233.
16. Chung CY, et al. (2013) Identification and rescue of α-synuclein toxicity in Parkinson patient-derived neurons. *Science* 342(6161):983–987.
17. Tardiff DF, et al. (2013) Yeast reveal a "druggable" Rsp5/Nedd4 network that ameliorates α-synuclein toxicity in neurons. *Science* 342(6161):979–983.
18. Cooper AA, et al. (2006) Alpha-synuclein blocks ER-Golgi traffic and Rab1 rescues neuron loss in Parkinson's models. *Science* 313(5785):324–328.
19. Gitler AD, et al. (2008) The Parkinson's disease protein alpha-synuclein disrupts cellular Rab homeostasis. *Proc Natl Acad Sci USA* 105(1):145–150.
20. Outeiro TF, Lindquist S (2003) Yeast cells provide insight into alpha-synuclein biology and pathobiology. *Science* 302(5651):1772–1775.
21. Guzman JN, et al. (2010) Oxidant stress evoked by pacemaking in dopaminergic neurons is attenuated by DJ-1. *Nature* 468(7324):696–700.
22. Su LJ, et al. (2010) Compounds from an unbiased chemical screen reverse both ER-to-Golgi trafficking defects and mitochondrial dysfunction in Parkinson's disease models. *Dis Model Mech* 3(3-4):194–208.
23. Singleton AB, et al. (2003) alpha-Synuclein locus triplication causes Parkinson's disease. *Science* 302(5646):841.
24. Black DJ, Leonard J, Persechini A (2006) Biphasic Ca^{2+}-dependent switching in a calmodulin-IQ domain complex. *Biochemistry* 45(22):6987–6995.
25. Liu X, Yang PS, Yang W, Yue DT (2010) Enzyme-inhibitor-like tuning of $Ca^{(2+)}$ channel connectivity with calmodulin. *Nature* 463(7283):968–972.
26. Geiser JR, van Tuinen D, Brockerhoff SE, Neff MM, Davis TN (1991) Can calmodulin function without binding calcium? *Cell* 65(6):949–959.
27. Irwin DJ, et al. (2012) Neuropathologic substrates of Parkinson disease dementia. *Ann Neurol* 72(4):587–598.
28. Polymeropoulos MH, et al. (1997) Mutation in the α-synuclein gene identified in families with Parkinson's disease. *Science* 276(5321):2045–2047.
29. Breuder T, Hemenway CS, Movva NR, Cardenas ME, Heitman J (1994) Calcineurin is essential in cyclosporin A- and FK506-sensitive yeast strains. *Proc Natl Acad Sci USA* 91(12):5372–5376.
30. Hilioti Z, Cunningham KW (2003) The RCN family of calcineurin regulators. *Biochem Biophys Res Commun* 311(4):1089–1093.
31. Schreiber SL, Crabtree GR (1992) The mechanism of action of cyclosporin A and FK506. *Immunol Today* 13(4):136–142.
32. Cao S, Gelwix CC, Caldwell KA, Caldwell GA (2005) Torsin-mediated protection from cellular stress in the dopaminergic neurons of Caenorhabditis elegans. *J Neurosci* 25(15): 3801–3812.
33. Harrington AJ, Yacoubian TA, Slone SR, Caldwell KA, Caldwell GA (2012) Functional analysis of VPS41-mediated neuroprotection in Caenorhabditis elegans and mammalian models of Parkinson's disease. *J Neurosci* 32(6):2142–2153.
34. Lee JI, et al. (2003) The Caenorhabditis elegans homologue of Down syndrome critical region 1, RCN-1, inhibits multiple functions of the phosphatase calcineurin. *J Mol Biol* 328(1):147–156.
35. Piña FJ, et al. (2011) Hph1 and Hph2 are novel components of the Sec63/Sec62 posttranslational translocation complex that aid in vacuolar proton ATPase biogenesis. *Eukaryot Cell* 10(1):63–71.
36. Qureshi HY, Paudel HK (2011) Parkinsonian neurotoxin 1-methyl-4-phenyl-1,2,3,6-tetrahydropyridine (MPTP) and alpha-synuclein mutations promote Tau protein phosphorylation at Ser262 and destabilize microtubule cytoskeleton in vitro. *J Biol Chem* 286(7):5055–5068.
37. Fadri M, Daquinag A, Wang S, Xue T, Kunz J (2005) The pleckstrin homology domain proteins Slm1 and Slm2 are required for actin cytoskeleton organization in yeast and bind phosphatidylinositol-4,5-bisphosphate and TORC2. *Mol Biol Cell* 16(4):1883–1900.
38. deHart AK, Schnell JD, Allen DA, Tsai JY, Hicke L (2003) Receptor internalization in yeast requires the Tor2-Rho1 signaling pathway. *Mol Biol Cell* 14(11):4676–4684.
39. Cyert MS (2003) Calcineurin signaling in Saccharomyces cerevisiae: How yeast go crazy in response to stress. *Biochem Biophys Res Commun* 311(4):1143–1150.
40. Picotti P, et al. (2010) High-throughput generation of selected reaction-monitoring assays for proteins and proteomes. *Nat Methods* 7(1):43–46.
41. Roy J, Li H, Hogan PG, Cyert MS (2007) A conserved docking site modulates substrate affinity for calcineurin, signaling output, and in vivo function. *Mol Cell* 25(6):889–901.
42. Liu Q, et al. (2012) Selective ATP-competitive inhibitors of TOR suppress rapamycin-insensitive function of TORC2 in Saccharomyces cerevisiae. *ACS Chem Biol* 7(6):982–987.
43. Aramburu J, et al. (1999) Affinity-driven peptide selection of an NFAT inhibitor more selective than cyclosporin A. *Science* 285(5436):2129–2133.
44. Stathopoulos AM, Cyert MS (1997) Calcineurin acts through the CRZ1/TCN1-encoded transcription factor to regulate gene expression in yeast. *Genes Dev* 11(24):3432–3444.
45. Doty RL (2012) Olfactory dysfunction in Parkinson disease. *Nat Rev Neurol* 8(6):329–339.
46. Lin X, et al. (2009) Leucine-rich repeat kinase 2 regulates the progression of neuropathology induced by Parkinson's-disease-related mutant alpha-synuclein. *Neuron* 64(6):807–827.
47. Armstrong RA, et al. (2014) A quantitative study of α-synuclein pathology in fifteen cases of dementia associated with Parkinson disease. *J Neural Transm* 121(2):171–181.
48. Chartier-Harlin MC, et al. (2004) Alpha-synuclein locus duplication as a cause of familial Parkinson's disease. *Lancet* 364(9440):1167–1169.
49. Butcher SP, Henshall DC, Teramura Y, Iwasaki K, Sharkey J (1997) Neuroprotective actions of FK506 in experimental stroke: In vivo evidence against an antiexcitotoxic mechanism. *J Neurosci* 17(18):6939–6946.
50. Kitamura Y, Itano Y, Kubo T, Nomura Y (1994) Suppressive effect of FK-506, a novel immunosuppressant, against MPTP-induced dopamine depletion in the striatum of young C57BL/6 mice. *J Neuroimmunol* 50(2):221–224.
51. Costantini LC, et al. (1998) A novel immunophilin ligand: Distinct branching effects on dopaminergic neurons in culture and neurotrophic actions after oral administration in an animal model of Parkinson's disease. *Neurobiol Dis* 5(2):97–106.
52. Guo X, Dawson VL, Dawson TM (2001) Neuroimmunophilin ligands exert neuroregeneration and neuroprotection in midbrain dopaminergic neurons. *Eur J Neurosci* 13(9):1683–1693.
53. Guo X, Dillman JF, 3rd, Dawson VL, Dawson TM (2001) Neuroimmunophilins: Novel neuroprotective and neuroregenerative targets. *Ann Neurol* 50(1):6–16.
54. Armistead DM, et al. (1995) Design, synthesis and structure of non-macrocyclic inhibitors of FKBP12, the major binding protein for the immunosuppressant FK506. *Acta Crystallogr D Biol Crystallogr* 51(Pt 4):522–528.
55. Steiner JP, et al. (1997) Neurotrophic actions of nonimmunosuppressive analogues of immunosuppressive drugs FK506, rapamycin and cyclosporin A. *Nat Med* 3(4):421–428.
56. Meissner W, Hill MP, Tison F, Gross CE, Bezard E (2004) Neuroprotective strategies for Parkinson's disease: Conceptual limits of animal models and clinical trials. *Trends Pharmacol Sci* 25(5):249–253.
57. Tadross MR, Ben Johny M, Yue DT (2010) Molecular endpoints of Ca2+/calmodulin- and voltage-dependent inactivation of Ca(v)1.3 channels. *J Gen Physiol* 135(3):197–215.
58. Dick IE, et al. (2008) A modular switch for spatial Ca2+ selectivity in the calmodulin regulation of CaV channels. *Nature* 451(7180):830–834.
59. Bean BP (2007) Neurophysiology: Stressful pacemaking. *Nature* 447(7148):1059–1060.
60. Martinez J, Moeller I, Erdjument-Bromage H, Tempst P, Lauring B (2003) Parkinson's disease-associated alpha-synuclein is a calmodulin substrate. *J Biol Chem* 278(19): 17379–17387.
61. Lee D, Lee SY, Lee EN, Chang CS, Paik SR (2002) alpha-Synuclein exhibits competitive interaction between calmodulin and synthetic membranes. *J Neurochem* 82(5):1007–1017.
62. Mosharov EV, et al. (2009) Interplay between cytosolic dopamine, calcium, and alpha-synuclein causes selective death of substantia nigra neurons. *Neuron* 62(2):218–229.
63. Thayanidhi N, et al. (2010) Alpha-synuclein delays endoplasmic reticulum (ER)-to-Golgi transport in mammalian cells by antagonizing ER/Golgi SNAREs. *Mol Biol Cell* 21(11):1850–1863.
64. Nemani VM, et al. (2010) Increased expression of alpha-synuclein reduces neurotransmitter release by inhibiting synaptic vesicle reclustering after endocytosis. *Neuron* 65(1):66–79.
65. Gitler AD, et al. (2009) Alpha-synuclein is part of a diverse and highly conserved interaction network that includes PARK9 and manganese toxicity. *Nat Genet* 41(3): 308–315.
66. Bodenmiller B, et al. (2010) Phosphoproteomic analysis reveals interconnected system-wide responses to perturbations of kinases and phosphatases in yeast. *Sci Signal* 3(153):rs4.

Supporting Information

Caraveo et al. 10.1073/pnas.1413201111

SI Materials and Methods

Mammalian Constructs. All neuronal constructs were cloned into the pLENTI6/V5 DEST (Invitrogen) lentivirus expression vector using the Gateway system. These included the genetic encoded sensor for calmodulin (CaM), $BSCaM_{IQ}$ as described above, β-galactosidase (LacZ), and α-synuclein (α-syn)A543T.

Rat Primary Cortical Cultures. Cultures were prepared based on Lesuisse and Martin (1). Embryos were harvested by Cesarean section from anesthetized pregnant Sprague–Dawley rats at embryonic day 18. Cerebral cortices were isolated and dissociated with ACCUMAX digestion for 20 min at 37 °C and trituration with Pasteur pipettes. Polyornithine and laminin-coated 96-well plates were seeded with 4×10^4 cells in neurobasal medium (Life Technologies) supplemented with B27 (Life Technologies), 0.5 mM glutamine, 25 μM β-mercaptoethanol, penicillin (100 IU/mL), and streptomycin (100 μg/mL). One-third of the medium was changed every 3–4 d. FK506 (Sigma) at the indicated concentrations was added to the lentivirus-transduced cultures in 96-well plates at day in vitro (DIV)18 keeping the amount of DMSO constant (vehicle). As a surrogate marker of cell viability, cellular ATP content was measured using the ViaLight Plus kit (Lonza). As a secondary method for quantitating neuronal toxicity, neurons were stained with an antibody specific for the neuronal marker microtubule-associated protein 2 (MAP2) (see details below).

Lentiviral constructs were packaged via lipid-mediated transient transfection of the expression constructs and packaging plasmids (pMD2.G and psPAX2) into 293 cells. Lentivirus were purified and concentrated using the Lenti-X Maxi Purification kit and LentiX Concentrator (Clontech) according to the manufacturer's protocol. Lentivirus titer was determined using the QuickTiter Lentivirus titer kit (lentivirus-associated HIV p24; Cell Biolabs) according to the manufacturer's protocol. Rat cortical cultures were transduced with various multiplicities of infection (MOI) of lentivirus at DIV5.

Immunocytochemistry and Quantification of Viable Neurons. For imaging, cells were cultured in PerkinElmer ViewPlates-96F tissue culture coated with polyornithine/laminin. For immunohistochemical staining, cells were rinsed with PBS, fixed in 4% (vol/vol) paraformaldehyde for 15 min, permeabilized, and blocked for 1 h in blocking buffer (PBS, containing 0.1% Triton X-100 and 10% normal donkey serum). Cells were then incubated with a rabbit polyclonal antibody against MAP2 (1:500; Millipore) in blocking buffer at 4 °C overnight. After the primary antibody incubation, cells were rinsed with PBS and incubated with secondary antibodies (Alexa Fluor 568 donkey anti-rabbit IgG (1:500; Invitrogen) for 1 h at room temperature. Subsequently, the neurons were rinsed three times with PBS, and nuclei were stained with Hoechst 33342 (Invitrogen) for 15 min and rinsed with PBS. Images were taken using an Eclipse Ti Nikon microscope (10× objective). The number of live neurons was determined by manually counting MAP2 and Hoechst-positive cells from 20 random fields per well, three wells per condition.

DA Neuronal Experiments. Ventral midbrains (VMs) from mice postnatal day 0–2 were dissected, dissociated, and plated on a monolayer of rat cortical astrocytes at a plating density of ∼100,000 cells per square centimeter, as previously described (2, 3). Neurons were cultured on glass poly-D-lysine–coated coverslips attached to ∼0.8-cm^2 wells cut into 50-mm dishes. Four–five d after plating, VM cultures were infected with the adeno-associated virus 2 virus carrying human A53T α-syn tagged with the red fluorescent tag mKate2. The virus was used at a 20,000 genome copies per cell concentration, resulting in >90% infection of dopaminergic (DA) neurons. After 7–14 d incubation with the virus, cultures were fixed and stained for tyrosine hydroxylase (TH) (see below), and the density of DA neurons assessed by counting the number of immunoreactive cells in 20 random fields of view at 200× magnification (Plan-Neofluar 20× objective; ∼0.8 mm2 viewing field) and taking the average as representative of each dish. Immunostaining of 4% paraformaldehyde-fixed cultures was performed using a mouse anti-TH (1:1,000; Chemicon) antibody followed by a secondary antibody conjugated with Alexa 488 (1:250; Molecular Probes).

Mouse and Human Brain Immunohistochemistry and Western Blot.
Mice. All protocols were approved by the Massachusetts Institute of Technology university administrative panel on laboratory animal care. C57BL6 α-syn A53T were obtained from The Jackson Laboratory donated by Huaibin Cai's laboratory. In our hands, this colony did not show clear signs of neurodegeneration until 8 mo of age.

For Western blot (WB) procedures, mice brains were homogenized with lysis buffer (1 mL for 250 mg of tissue; 40 mM Hepes, 120 mM NaCl, and 0.3% CHAPS) supplemented with protease and phosphatase inhibitors (1× Roche complete protease inhibitor mixture). Crude extracts were cleared at 13,000 rpm for 20 min and 20 μg of protein was loaded onto a denaturing gel. Primary antibodies were anti-PKCα (1:500; Santa Cruz Biotechnology, sc-208) and anti-S657 PKCα (1:500; Santa Cruz Biotechnology, sc-12356).

Human samples. Archival formalin-fixed, paraffin-embedded brain tissue (frontal cortex, hippocampus, amygdala, and midbrain) was obtained from the Massachusetts Alzheimer Disease Research Center. Five-micrometer tissue sections were immunostained with primary antibody overnight at 4 °C, followed by secondary antibody, avidin-biotin Complex incubation (Vectastain ABC Elite kit; Vector Laboratories), and developing with ImmPACT 3,3′-diaminobenzidine peroxidase substrate (Vector Laboratories). Primary antibodies used were rabbit polyclonal against nuclear factor of activated T cells (NFAT) (anti-NFATc4) (1:250; Santa Cruz Biotechnology, sc-32985) and mouse monoclonal anti-NFATc3 (1:400; Santa Cruz Biotechnology, sc-8405). NFATc4 competing peptide was added before the primary antibody NFATc4, according to the manufacturer's instructions (1:4,000; Santa Cruz Biotechnology, sc-1149).

Calcium Imaging in Rat Cortical Neurons. Neurons in eight-well chambered coverglass (D-lysine 2 mg/mL; Sigma) and mouse laminin (1 mg/mL; BD Biosciences) were incubated in Tyrode's solution (129 mM NaCl, 5 mM KCl, 2 mM $CaCl_2$, 1 mM $MgCl_2$, 25 mM Hepes, 30 mM glucose, pH 7.4) containing 5 μM Fluo4 acetoxymethyl (AM) ester (Invitrogen, diluted in Tyrode's from 4.55 mM fresh stock in DMSO/20% Pluronic F-127) for 45 min in the dark at 37 °C. The solution was changed and the cells were incubated for an additional 15 min in Tyrode's at room temperature to allow deesterification. Imaging was conducted using a TE-2000S inverted microscope with an environment chamber at room temperature and 5% (vol/vol) CO_2. With a standard FITC excitation filter, time series images were captured using a Photometrics CoolSnap EZ camera controlled by the NIS-Elements AR software package. Time series experiments consisted

of 600 512 × 512 frames with an interval of 1 s. After a baseline interval of ∼200 frames, high KCl Tyrode's solution was added to the well for a final KCl concentration of 30 mM. Image stacks were exported to ImageJ (National Institutes of Health, NIH), fluorescence intensities were measured, and data were exported to and analyzed in Excel (Microsoft). Measurements shown represent deltaF = F/Fo (increase in fluorescence over baseline following background subtraction). Each trace represents the normalized fluorescence intensity change of one cell over time. Cells were assigned by mKate positivity.

Calcium Imaging in Yeast. Intracellular calcium was measured using the 2μ plasmid PEV11/AEQ (kindly provided by Martha Cyert, Stanford University, Stanford, CA) as a calcium probe. Briefly, yeast cells were grown to log phase in synthetic defined (SD) media, switched to S-raffinose media at a starting OD_{600} = 0.0035 overnight, and finally switched to S-galactose media at a starting OD_{600} = 0.1–0.3 to induce the expression of α-syn. At the indicated time points, samples were harvested and resuspended in fresh galactose media containing 5.9 mM coelenterazine (Invitrogen) and rotated at room temperature for 60 min. Yeast were washed once in coelenterazine-free media, resuspended in a final volume of 300 mL, and transferred to luminometer tubes. Luminescence was recorded using a Berthold LB953 luminometer and reported as relative luminescence units per second. Experiments were performed in duplicate with at least three independent replicates. For the experiments regarding calcium chelators, yeast were induced in galactose-containing media as described above in the presence of ethylene glycol tetraacetic acid (EGTA; Sigma) and/or the presence of 1,2-bis(*o*-aminophenoxy) ethane-*N,N,N,N*-tetraacetic acid (BAPTA-AM; Invitrogen) for 5 h. Samples were then processed with coelenterazine as outlined above.

Propidium Iodide Staining. Yeast strains used for calcium imaging were assayed in parallel for propidium iodide (PI) staining. Briefly, cells induced in galactose media were incubated with 20 μg/mL PI for 15 min at room temperature, washed with water, and PI-positive cells counted on a flow cytometer (Guava System) using the FL-2 channel.

Yeast Cell Lysis. Yeast strains were grown in synthetic media lacking the selected auxotrophic markers in either glucose or rafinose media overnight at 30 °C. Cultures were then diluted into the same media and/or inducing media to an OD_{600} of 0.2 and grown for 4 h. Cells were spun down for 5 min at 1,000 × *g*. Yeast pellets were resuspended in 200 μL ethanol lysis buffer with 3 mM PMSF. To this solution, 200 μL of glass beads was added and the mixture vortexed for 3 min on maximum speed at 4 °C; samples were subsequently frozen at −80 °C overnight. To evaporate the ethanol, samples were subjected to speed vacuum for 20 min and reconstituted in 200 μL of 2% SDS buffer, boiled for 5 min, spun down, and supernatants were collected for protein quantitation using a bicinchoninic (BCA) assay (Pierce).

Western Blot Procedure. Once normalized to equal amounts of protein, samples were loaded into a 4–12% Bis-Tris gel (Invitrogen) and run at 150 V for 50 min. The gel was then transferred to a 0.2 μ PVDF membrane (Bio-Rad) in a methanol-based buffer for 2 h at 400 mA constant current. The membrane was blocked with 5% milk in PBS/Tween 0.5% for 1 h at room temperature and subsequently washed three times for 5 min each time in PBS/Tween 0.5%. The membrane was incubated with rabbit anti-aequorin antibody (Abcam) at a 1:1,000 dilution in PBS/Tween 0.5% for 1 h at room temperature. The membrane was washed three times as previously described and subsequently incubated with anti-rabbit secondary antibody (DyLight; Rockland) at a 1:10,000 dilution in PBS for 1 h. The membrane was washed in PBS three times for 5 min each time and scanned using a Licor Odyssey Scanner.

Yeast Constructs and Transformations. All transformations in yeast either for deletion and/or for overexpression purposes were performed at least three independent times and analyzed with at least three independent transformants each time. All yeast constructs were cloned into the Gateway entry vector pDONR221 and then moved to expression vectors containing pAG416GPD and Gal and/or pAG415GPD and Gal. The $BSCaM_{IQ}$ construct contains the rat neuromodulin IQ domain (MAATKIQAAFR-GHITRKKLKDEKKGASRGPYSIVSPKC) flanked by yellow fluorescent protein (YFP) at the N terminus and cyanide fluorescent protein (CFP) at the C terminus. The CY_{IQ} construct contains YFP at the N terminus and the rat myosin light chain type 1C IQ domain (MAATQIQAAFRGPITRKKLKDEKKG-ASRGPYSIVSPKC). CaM_{1-4} corresponds to the rat calmodulin with the following point mutations: D68A, D184A, D301A, and D357A. $CaMEF_1$ corresponds to the yeast calmodulin with mutations D21A and E32V in the first EF hand. $CaMEF_2$ corresponds to the yeast calmodulin with mutations D57A and E68V in the second EF hand. $CaMEF_3$ corresponds to the yeast calmodulin with mutations D94A and E105V in the third EF hand. The other overexpression constructs were obtained from the 2005 FLEXGene library and include: calmodulin, Rcn1, Rcn2, Hph1, Slm2, and Crz1. The 4 copies of the Crz1-dependent responsive element (4X-CDRE) as well as the Crz1-PVIVIT constructs were a kind gift from Martha Cyert (Stanford University) (4).

Spotting Assays. Cells were grown overnight at 30 °C in 3 mL SD media lacking the relevant amino acids and containing glucose. Cell concentrations (OD_{600}) were adjusted to the lowest concentration and then fivefold serially diluted and spotted onto SD media plates containing glucose (uninduced) or galactose (induced). Plates were incubated at 30 °C for 2 (glucose) or 3 d (galactose).

Yeast Deletions. All deletions were performed by homologous recombination according to the *Saccharomyces* Genome Deletion Project using a one-step gene disruption. Briefly, a PCR-based strategy was performed to amplify a product that contains an antibiotic resistance cassette (either kanamycin or hygromycin) flanked by 45 base pairs (bp) of sequence corresponding to the 5′ and 3′ UTR of the target gene (sequence available at the *Saccaromyces* Genome Deletion Project). Yeast strains were transformed with the PCR product using a standard lithium acetate protocol, allowed to recover overnight in YPD media at 30 °C, and then selected on plates with the corresponding antibiotic-resistant marker. Colonies were screened for the deletion using PCR confirmation primers. Results are representative of at least three independent colonies.

Mutagenesis. Mutations were introduced using the QuikChange XL site-directed mutagenesis kit (Stratagene), with yeast CaM as a template. To generate the calmodulin single EF hand mutants, we used yeast calmodulin as a template. For CaM_{EF1} the mutagenic primers were 5′-CTCTTTGCTAAGAAGTGTTTTGG-CC-3′ (forward) and 5′-GGCCAATACACTTCTTTAGCAAA-GAG-3′ (reverse). For CaM_{EF2} the mutagenic primers were 5′-CGAAATAGCTGTTGTGTATTTTTGGC -3′ (forward) and 5′-GCCAAAAATACACAACAGCTATTTCG-3′ (reverse). For the CaM_{EF3} the mutagenic primers were 5′-GTATTCGCTAAGA-CGCTGTGTTGAAA-3′ (forward) and 5′-TTTCAACACAGC-GTCTTAGCGAATAC-3′ (reverse). For all EF hand mutants the PCR was carried out as follows: 1 cycle at 95 °C for 1 min; 18 cycles of 95 °C for 30 s, 55 °C for 1 min, and 68 °C for 7 min 30 s; and 1 cycle at 68 °C for 7 min 30 s.

CDRE Reporter Assay. Control and HiTox strains were transformed with the 4×-CDRE::*lacZ* reporter construct. Cells were grown and induced as described for the yeast calcium assays and assayed for β-galactosidase activity using a Promega luciferase kit 9 h after α-syn induction.

FRET Experiments. An aliquot of 1 mL of yeast cells (control and HiTox strains) grown in inducing media (galactose) to OD_{600} = 0.2 were spun down and resuspended in 10 μL of water to maintain a uniform density of cells. The 1-μL droplets of resuspended cells, placed onto 3.5-cm culture dishes, were allowed to sediment for 10 min. Aggregate cyan fluorescent protein (CFP) (S_{CFP}; excitation Chroma D440/20X; emission D480/30M) and "FRET" (S_{FRET}; excitation Chroma 436/20X; emission Chroma D535/30M) fluorescence measurements were obtained from the center of such droplets using a Nikon TE3000 microscope (40 × 1.3 NA objective) and a custom fluorometer (5, 6). Autofluorescence was estimated and subtracted from both S_{CFP} and S_{FRET} measurements at each time point for both strains. Subsequently, the ratio $R(t) = S_{FRET}/S_{CFP}$ was computed for each droplet at each time point. For the $BSCaM_{IQ}$ sensor in yeast cells, we estimated $R_{min} = 0.53$ and $R_{max} = 2.20$. Relative $[CaM]_{free}$ is estimated as

$$\frac{[CaM]_{free}(t)}{[CaM]_{free}(0)} = \left(\frac{R_{max} - R(t)}{R(t) - R_{min}}\right)\left(\frac{R(0) - R_{min}}{R_{max} - R(0)}\right).$$

Selected Reaction Monitoring- Based Mass Spectrometry. ***Protein extraction from cell pellets.*** Strains were grown for 16 h on α-syn induction media and precipitated with 6.25% final volume of trichloroacetic acid. Supernatants were discarded after centrifugation (1,500 × *g*, 4 °C, 5 min) and resuspended with 10 mL of cold acetone. Supernatants were again discarded after centrifugation (1,500 × *g*, 4 °C, 5 min) and resuspended with 1 mL of cold acetone. A final centrifugation step was carried out before drying the pellets. Dry cell pellets were resuspended in cell lysis buffer (8 M urea, 0.05 M ammonium bicarbonate, and 0.005 M EDTA). The suspension was flash frozen in liquid nitrogen and acid-washed glass beads were added at a 1:1 ratio with the cell pellet volume. Bead beating on a vortexing device was done six times for 10 min at 4 °C, adding new cell lysis buffer, centrifuging the samples at 5,000 × *g* for 5 min and collecting the supernatant each time. The total protein content of the pooled supernatant was assessed by BCA assay (Thermo Scientific) according to the manufacturer's instructions.

Tryptic digestion of protein extracts. A total of 2.5 mg of each protein extract was used for tryptic digestion. Disulfide bonds were reduced and alkylated with 10 mM tris(2-carboxyethyl)phosphine hydrochloride for 30 min at 32 °C and 40 mM iodoacetamide for 45 min at 25 °C in the dark, respectively. Samples were diluted with 0.1 M ammonium bicarbonate to a final concentration of 1 M urea and sequencing-grade porcine trypsin (Promega) was added to a final enzyme:substrate ratio of 1:100. Tryptic digestion was conducted overnight at 30 °C. The digestion was stopped by acidification with formic acid to 2%. The peptide mixtures were loaded onto Sep-Pak tC18 cartridges (Waters), desalted, and eluted with 80% acetonitrile (ACN). Peptide samples were evaporated on a vacuum centrifuge and stored dry at −20 °C.

Phosphopeptide enrichment. Dry peptide samples were resolubilized in phosphopeptide enrichment buffer (PEB) composed of 10% (m/v) phthalic acid, 80% ACN, and 0.1% trifluoroacetic acid (TFA). A total of 2.5 mg of TiO_2 resin (GL Sciences) per sample was used to enrich phosphopeptides according to the protocol described in ref. 7. Phosphopeptide samples were loaded on to Sep-Pak tC18 cartridges, desalted, and eluted with 50% ACN. Phosphopeptide samples were evaporated on a vacuum centrifuge until dry and then resolubilized in 12.5 μL of 0.1% TFA before analysis by mass spectrometry.

Selected reaction monitoring assay development. Selected reaction monitoring (SRM) assays were developed, using a previously described approach (8), for phosphopeptides from Slm2 and Crz1. Phosphopeptide sequences from these proteins were selected based on an in-house LC-MS/MS dataset. Crude heavy-isotope–labeled synthetic versions of the phosphopeptides were synthesized (Thermo Fischer Scientific Biopolymers) and SRM transitions for these targets were calculated using Skyline (v1.4, MacCoss Lab Software). For each synthetic peptide, we retained the eight most intense fragment ions from the most intense precursor ion and annotated the peptide retention times. These SRM coordinates were subsequently used for quantifying endogenous phosphopeptides. Peptide samples were separated by online liquid chromatography and measured on a triple quadrupole/ion trap mass spectrometer (5500 QTrap; AB SCIEX) according to the settings described (9). SRM analysis was conducted with a dwell time of 10 ms and a cycle time of <2.5 s for unscheduled runs, and a retention time window of 5 min and a target cycle time of 2.5 s for scheduled runs. Target peptide realignment for scheduled SRM was accomplished using the iRT kit (Biognosys) according to the manufacturer's instructions.

Phosphopeptide quantification by SRM. Endogenous phosphopeptide mixtures (3 μL) from α-syn–expressing yeast with and without FK506 treatment were analyzed by scheduled SRM based on the eight most intense transitions for each target. Data were analyzed with Skyline and the top four to five transitions per peptide with no obvious interferences were retained for quantification. Peak intensities of the transitions were used for quantification after confirming coelution, peak shape similarity, and relative transition ratios compared with the respective synthetic peptide reference. Relative phosphopeptide abundance was calculated as the average of the transition intensities in each sample versus control; therefore, control samples are shown to have a relative abundance of 1. The standard deviation was calculated from technical and biological variability in using five different transitions and two biological replicates to measure the phosphopeptide, ENVDS(phospho)PR from SLM2 and four different transitions to measure the phosphopeptide, MDSANSS(phospho)EKISK from CRZ1. Both peptides were unique to the sequence of the corresponding protein.

RNAi in *Caenorhabditis elegans*. RNAi feeding clones (Geneservice) were isolated and grown overnight in LB media with 100 μg/mL ampicillin. Nematode growth media plates containing 1 mM isopropyl β-D-1-thiogalactopyranoside were seeded with RNAi feeding clones and double-stranded RNA was induced overnight at room temperature. Adult hermaphrodites were transferred to corresponding RNAi plates and allowed to lay eggs for 5 h to synchronize the F1 progeny. The dopaminergic neurons in the F1 progeny were analyzed at day 6 for degeneration.

Cell-Specific RNAi in *C. elegans*. Transgenic *C. elegans* lines were generated by directly injecting the expression plasmid $P_{dat\text{-}1}$::*sid-1* along with the phenotypic marker $P_{myo\text{-}2}$::mCherry (pharyngeal expression) (Addgene) into *sid-1(pk3321)* hermaphrodites to create stable transgenic animals expressing genomic *sid-1* in the dopaminergic neurons as well as the phenotypic marker (mCherry) in the pharynx. The extrachromosomal array ($P_{dat\text{-}1}$::*sid-1*, $P_{myo\text{-}2}$::mCherry) was integrated into the *C. elegans* genome by UV irradiation (10) to create strain UA195 [*sid-1(pk3321); baIn33* ($P_{dat\text{-}1}$::*sid-1*, $P_{myo\text{-}2}$::mCherry)]. Integrated transgenic lines were outcrossed with *sid-1(pk3321)* nematodes five times to remove any extraneous mutations. The isolated homozygous integrated lines were crossed into strain UA44 [*baIn11* ($P_{dat\text{-}1}$::α-syn, $P_{dat\text{-}1}$::GFP)] to generate strain UA196 [*sid-1(pk3321);baIn11; baIn33*], which expresses α-syn, GFP, and SID-1 in the dopaminergic

neurons and is susceptible to RNAi selectively in these specific neurons. UA202 [*sid-1(pk3321);* P_{dat-1}::GFP*; baIn36* P_{dat-1}*:: sid-1*, P*myo-2*::mCherry)] acts as a control strain for UA196.

***C. elegans* RCN-1 Overexpression and Quantitation.** *C. elegans rcn-1* gene was amplified using iProof high-fidelity DNA polymerase (Bio-Rad) from genomic DNA isolated from N2 Bristol nematodes. The primers were designed according to the sequence information from WormBase (www.wormbase.org), and a HA tag was added to the C-terminal of *rcn-1*. The *rcn-1* construct was cloned into Gateway (Invitrogen) entry vector pDONR221 and then shuttled into worm Gateway expression vector pDEST-DAT-1 (11). The *rcn-1* construct was verified by DNA sequencing before introduced into worms by microinjection.

Transgenic worms were generated by injecting plasmid construct (P_{dat-1}::*rcn-1*, 5 ng/μL), along with a phenotypic marker (P_{unc-54}::tdTomato, 50 ng/μL, body wall muscle expression), into worm strain UA44 [*baIn11* (P_{dat-1}::α-syn, P_{dat-1}::GFP)] or BY250 [vtls7 (P_{dat-1}::GFP)] to create multiple stable transgenic lines, UA252-1/2/3/4 [*baEx143*-1/2/3/4(Pdat-1::rcn-1, Punc-54::tdTomato), baIn11] and UA253-1/2/3/4 [*baEx144*-1/2/3/4 (Pdat-1::rcn-1, Punc-54::tdTomato), vtIs7], which express various levels of *rcn1* in the dopaminergic neurons as detected by the phenotypic red marker in the body wall muscle cells. The *rcn-1* transcription level in the transgenic worm lines was measured by semi-quantitative RT-PCR and the transgenic worms were further analyzed for dopaminergic neurodegeneration. Total RNA was isolated from 100 young adult hermaphrodite worms as previously described (12). The worms were transferred into 10 μL of M9 buffer and frozen at −80 °C for 1 h. After thawing, 100 μL of TRI reagent (Molecular Research Center) was added to the samples and incubated for 10 min at room temperature. The samples were freeze thawed four times in liquid N2, vortexed for 15 s with 10 μL of 1-bromo-3-chloropropane (Acros Organics), incubated for 10 min at room temperature, and centrifuged for 15 min at 14,100 × *g* at 4 °C. The supernatant was transferred to an RNase-free tube, mixed with 1.5 μL of glycoblue (Ambion) and 50 μL of −20 °C prechilled isopropanol, and stored overnight a −20 °C. The next day, the sample was centrifuged for 15 min at 14,500 rpm at 4 °C and the supernatant was discarded. The pellet was washed with 100 μL of RNase-free ethanol (75%) and resuspended in 10 μL of diethylpyrocarbonate-treated water. The sample was treated with 1 μL of DNase I (Promega) for 15 min at 37 °C, then with DNase Stop for 10 min at 65 °C. RT-PCR was performed using SuperScript III RT (Invitrogen) using oligo $(dT)_{20}$ primer following the manufacturer's protocol. cDNA amplification was performed using iProof high-fidelity DNA polymerase with primers specific for *rcn-1* or *ama-1* (internal control, encodes a subunit of RNA polymerase II, which is required for mRNA transcription). For *rcn-1* construct, the 3′ HA primer was used to specifically amplify the *rcn-1* transgene. Amplified products were separated on 1.0% agarose gels and visualized using GelRed staining (Biotium). To compare amounts of mRNA among transgenic lines, DNA gels were scanned using a FujiFilm LAS-4000 digital imaging system and analyzed with Multi Gauge v.3.0 software. cDNA intensities were determined (i.e., *rcn-1* values were divided by the *ama-1* values) and then normalized to the value of the transgenic line, which showed the lowest level of *rcn-1* transcription. Three independent experiments were performed and analyzed by unpaired Student *t* test with Welch's correction.

Dopaminergic Neurodegeneration Analysis in *C. elegans*. *C. elegans* dopaminergic neurons were analyzed for degeneration as previously described (12). Briefly, in the calcineurin RNAi experiment, strain UA196 and strain UA202 treated with *tax-6* or control RNAi were synchronized, grown at 20 °C, and analyzed at day 6 of development; in the *rcn-1* overexpression experiment, transgenic worm strains expressing "low (or moderate)" levels of rcn-1 in the dopamine neurons, UA252-a/b and UA253-a/b, were synchronized, grown at 20 °C, and analyzed at day 7 of development. On the day of analysis, the six anterior dopaminergic neurons [four CEP (cephalic) and two ADE (anterior deirid)] were examined in 30 adult hermaphrodite worms, which were immobilized on glass coverslips using 3 mM levamisole and transferred onto 2% agarose pads on microscope slides. Worms were considered normal when all six anterior neurons were present without any signs of degeneration, as previously reported (11, 12). In total, at least 90 adult worms were analyzed for each RNAi treatment (30 worms per trial × 3 trials) and 90–150 adult worms were analyzed for each independent *rcn-1* transgenic line (30 worms per trial, three to five independent trials). Statistical analyses were performed as Student *t* test when separate controls were used for each control-experimental set of conditions. Conversely, when multiple experimental conditions were compared with the same control, a one-way ANOVA, followed by a Tukey's post hoc analysis was performed.

1. Lesuisse C, Martin LJ (2002) Long-term culture of mouse cortical neurons as a model for neuronal development, aging, and death. *J Neurobiol* 51(1):9–23.
2. Burke RE, Antonelli M, Sulzer D (1998) Glial cell line derived neurotrophic growth factor inhibits apoptotic death of postnatal substantia nigra dopamine neurons in primary culture. *J Neurochem* 71(2):517–525.
3. Rayport S, Sulzer D (1995) Visualization of antipsychotic binding to living mesolimbic neurons reveals D2 receptor mediated, acidotropic and lipophilic components. *J Neurochem* 65(2):691–703.
4. Stathopoulos AM, Cyert MS (1997) Calcineurin acts through the CRZ1/TCN1-encoded transcription factor to regulate gene expression in yeast. *Genes Dev* 11(24):3432–3444.
5. Erickson MG, Alseikhan BA, Peterson BZ, Yue DT (2001) Preassociation of calmodulin with voltage-gated Ca(2+) channels revealed by FRET in single living cells. *Neuron* 31(6):973–985.
6. Erickson MG, Liang H, Mori MX, Yue DT (2003) FRET two-hybrid mapping reveals function and location of L-type Ca2+ channel CaM preassociation. *Neuron* 39(1):97–107.
7. Bodenmiller B, et al. (2010) Phosphoproteomic analysis reveals interconnected system-wide responses to perturbations of kinases and phosphatases in yeast. *Sci Signal* 3(153):rs4.
8. Picotti P, et al. (2010) High-throughput generation of selected reaction-monitoring assays for proteins and proteomes. *Nat Methods* 7(1):43–46.
9. Di Girolamo F, Lante I, Muraca M, Putignani L (2013) The role of mass spectrometry in the "omics" era. *Curr Org Chem* 17(23):2891–2905.
10. Inoue T, Thomas JH (2000) Targets of TGF-β signaling in *Caenorhabditis elegans* dauer formation. *Dev Biol* 217(1):192–204.
11. Cao S, Gelwix CC, Caldwell KA, Caldwell GA (2005) Torsin-mediated protection from cellular stress in the dopaminergic neurons of Caenorhabditis elegans. *J Neurosci* 25(15):3801–3812.
12. Hamamichi S, et al. (2008) Hypothesis-based RNAi screening identifies neuroprotective genes in a Parkinson's disease model. *Proc Natl Acad Sci USA* 105(2):728–733.

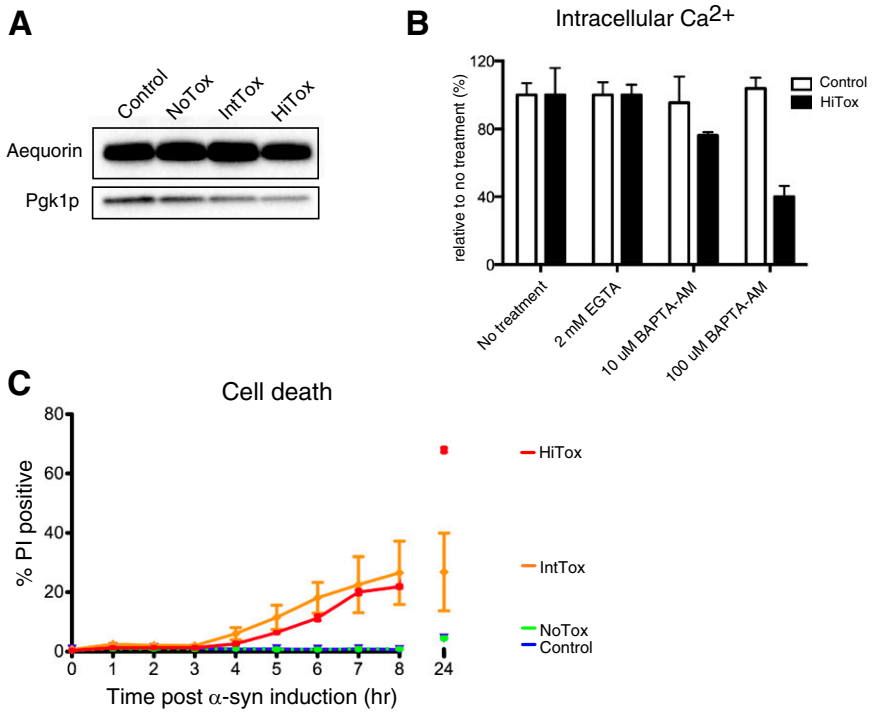

Fig. S1. Overexpression of α-syn is associated with increased cytosolic Ca^{2+}. (*A*) Control (no α-syn), NoTox (low copy number of α-syn), IntTox (intermediate copy number of α-syn), and HiTox (high copy number of α-syn) strains were transformed with aequorin, a genetically encoded Ca^{2+} indicator, and aequorin protein expression was assayed by Western blot (Pgk1p is used as a loading control). (*B*) Cytosolic Ca^{2+} in control and in HiTox strains 5 h after α-syn induction in the presence of 10 or 100 μM of the intracellular Ca^{2+} chelator BAPTA-AM or the extracellular Ca^{2+} chelator EGTA. Intracellular Ca^{2+} is reported relative to no treatment for each strain. (*C*) The same strains as in (Fig. 1*A*) were subjected in parallel to a time course for cell death measured by propidium iodide incorporation. Results are expressed as percentage of propidium iodide positive cells.

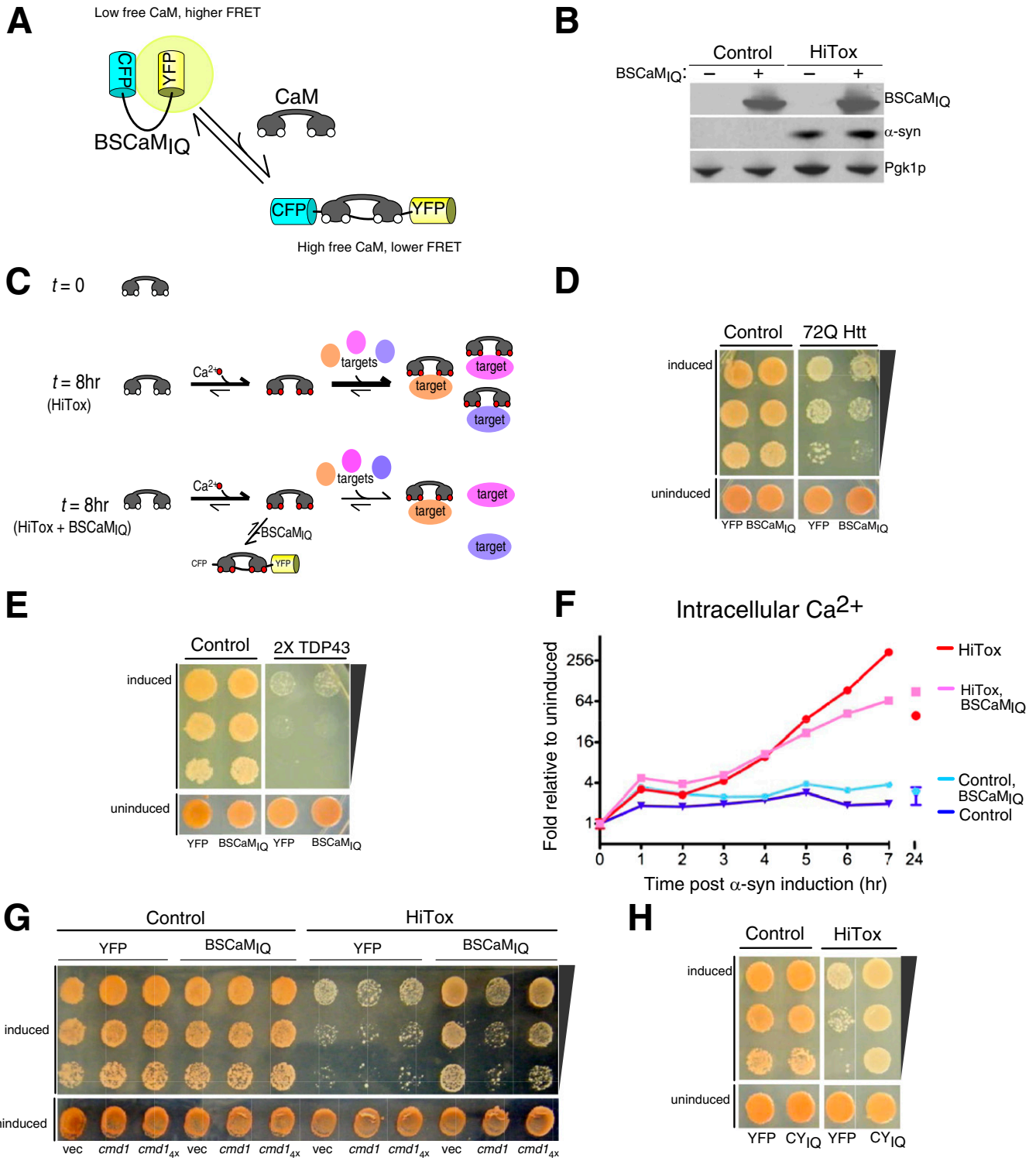

Fig. S2. $BSCaM_{IQ}$ and CY_{IQ} rescue toxicity induced by α-syn. (*A*) Schematic of $BSCaMI_Q$ composed of a calmodulin-binding domain flanked by cyan fluorescent protein (CFP) at the N terminus and yellow fluorescent protein (YFP) at the C terminus. CaM binding can be monitored by fluorescent resonance energy transfer (FRET). (*B*) Expression of both α-syn and $BSCaM_{IQ}$ in yeast assayed by Western blot (Pgk1p is used as a loading control). (*C*) Hypothetical schematic representation of $BSCaM_{IQ}$ acting as sink for calmodulin (CaM). (*D*) Yeast strains containing 72QHtt were spotted onto plates containing uninducing media (SD –Ura, 72Q Htt selective; *Lower*) and replica plated in threefold serial dilutions onto inducing plates containing selective media and SGal –Ura (*Upper*). (*E*) Yeast strains containing different levels of TDP43 were spotted onto plates containing uninducing media (SD –Ura, TDP43 selective; *Lower*) and replica plated in threefold serial dilutions onto inducing plates containing selective media and SGal –Ura (*Upper*). (*F*) Time course for cytosolic Ca^{2+} (measured by aequorin luminescence) after α-syn induction in control and HiTox strains in the presence and absence of $BSCaM_{IQ}$. (*G*) Yeast strains were spotted onto plates containing uninducing media (SD –Ura, Leu; $BSCaM_{IQ}$ and *cmd1* selective; *Lower*) and replica plated in threefold serial dilutions onto inducing plates containing selective media and (SGal –Ura, Leu) (*Upper*). Empty vector (vec) is used as control plasmid. *cmd1* = yeast calmodulin and $cmd1_{4X}$ = D68A, D184A, D301A, and D357A, a rat CaM mutant unable to bind calcium at all four EF hands. (*H*) Yeast strains containing CY_{IQ} were spotted onto plates containing uninducing media (SD –Ura, CY_{IQ} selective; *Lower*) and replica plated in threefold serial dilutions onto inducing plates containing selective media and SGal –Ura (*Upper*); YFP serves as control.

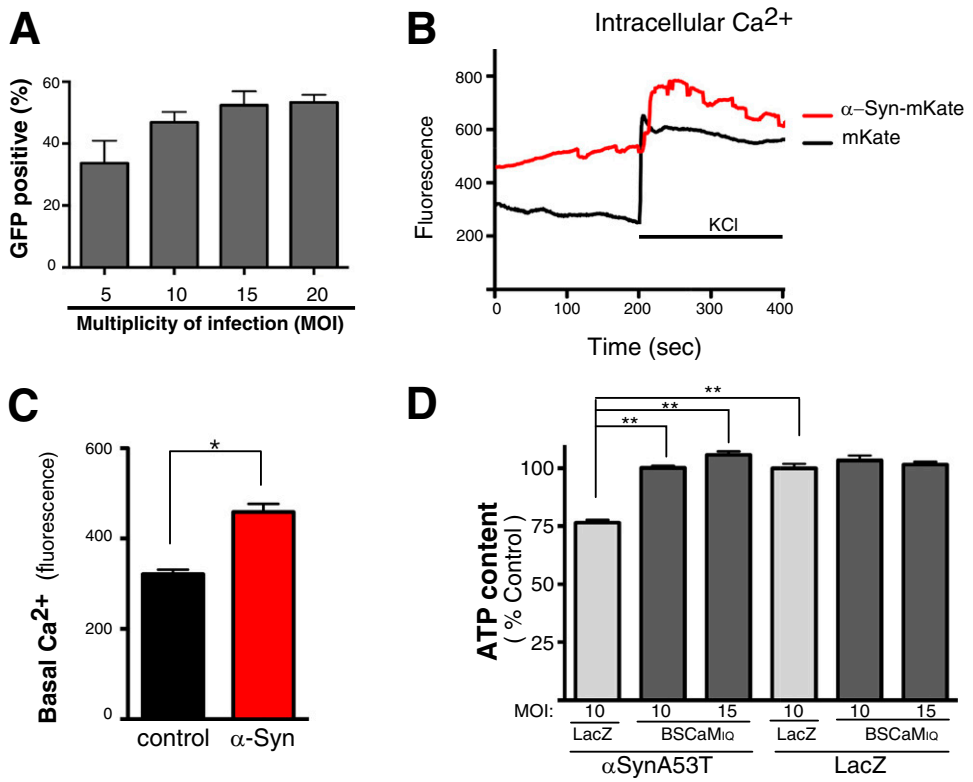

Fig. S3. Overexpression of α-syn increases intracellular Ca^{2+} in neurons. (*A*) α-synA53T-GFP infection efficiency on mouse cortical neurons expressed as percentage of positive neurons. (*B*) Rat primary neuronal cultures were infected with lentiviruses carrying mKate as a control or α-synA53T-mKate. Cytosolic Ca^{2+} was measured by luminescence using Fluo-4 before and after stimulation with 60 mM KCl. These traces are representative of two independent experiments each representing an average of ~20 cells. (*C*) From the cultures described in *B*, 45–60 cells were quantified for their basal cytosolic Ca^{2+} (nonstimulated condition) in control (m-Kate infected, black bar) and α-syn infected neurons (red bar). $^*P < 0.05$ (Student *t* test). (*D*) ATP content of cells remaining on the dish as a measure of viability. Data where normalized to control (LacZ infected) in the conditions described in *B*. $^*P < 0.05$, one-way ANOVA, Dunnett's multiple comparison test.

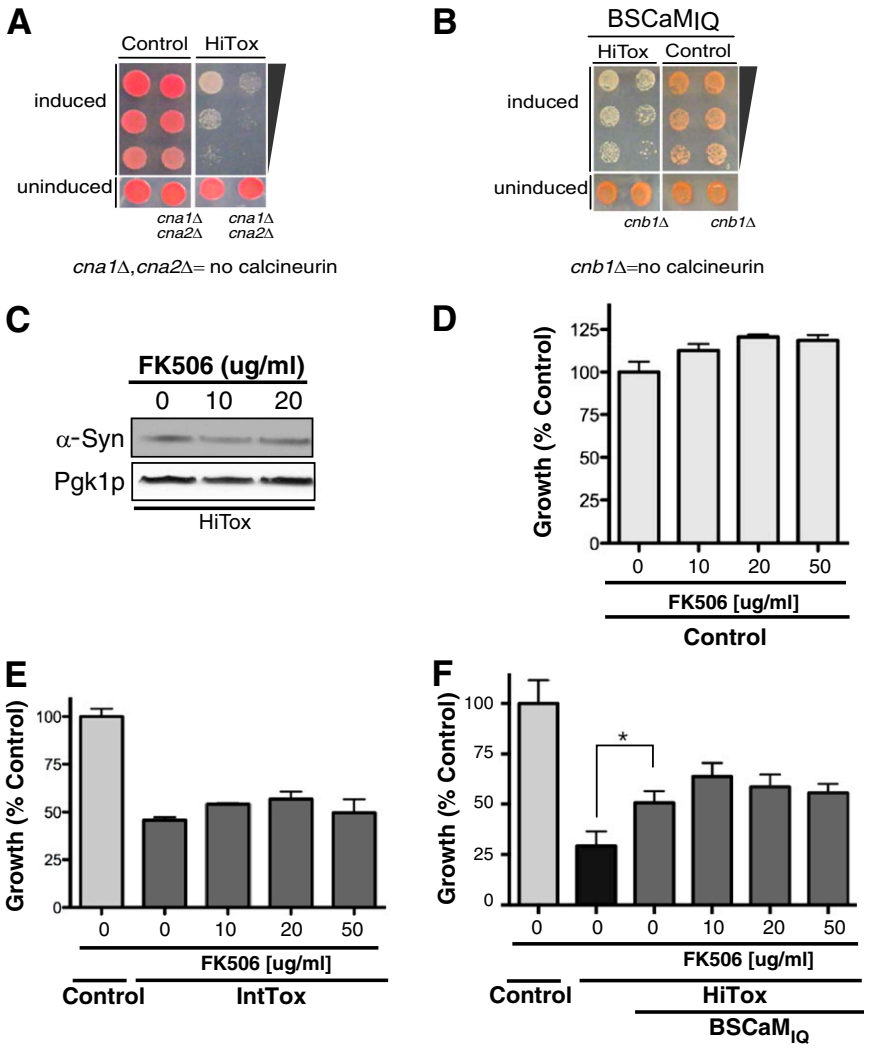

Fig. S4. Calcineurin activation is central to α-syn toxicity in yeast. (*A*) Control and HiTox strains with or without (*cna1*Δ, *cna2*Δ) calcineurin were spotted onto plates containing uninducing media (SD −His,Trp, α-syn selective; *Lower*) and replica plated in threefold serial dilutions onto α-syn–inducing plates containing selective media SGal (*Upper*). (*B*) Control and HiTox strains lacking calcineurin (*cnb1*Δ) were spotted onto plates containing uninducing media (SD −Ura $BSCaM_{IQ}$ selective; *Lower*) and replica plated in threefold serial dilutions on α-syn–inducing plates containing selective media SGal (*Upper*). (*C*) Expression of α-syn by Western blot in the HiTox strain in the presence of various FK506 concentrations (Pgk1p is used as a loading control). (*D*) Growth after 48 h of control strain relative to no drug over a range of FK506 concentrations (related to Fig. 2). (*E*) Growth (described as percentage over control) of IntTox cells grown for 48 h over a range of FK506 concentrations. (*F*) Growth (described as percentage over control) of HiTox cells w/o $BSCaM_{IQ}$ grown for 48 h over a range of FK506 concentrations.

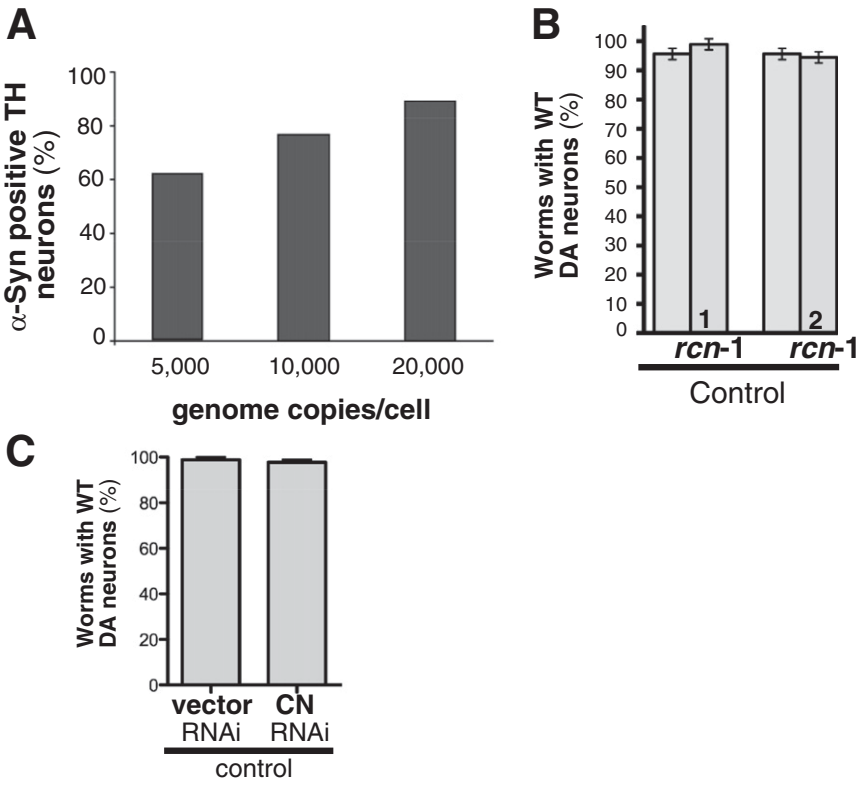

Fig. S5. Manipulations in calcineurin have no effect on viability of neurons from control *C. elegans*. (*A*) α-synA53T-mKate infection efficiency on mouse dopaminergic neurons expressed as percentage of TH positive neurons (related to Fig. 3). (*B*) Population of worms remaining with WT (wild type) numbers of dopaminergic neurons overexpressing *rcn-1* in control worms which lack α-syn (UA253-1/2). These animals were scored at day 7 of development. For each experiment, three independent experiments were performed, with 30 worms per trial ($P > 0.05$, one-way ANOVA). (*C*) Population of worms remaining with WT (wild type) numbers of neurons after treatment with RNAi for calcineurin/*tax-6* (CN) or empty vector RNAi control in GFP-expressing worms (UA202). These animals were scored at day 6 of development. For each experiment, three independent experiments were performed, with 30 worms per trial. *$P < 0.05$ (Student *t* test).

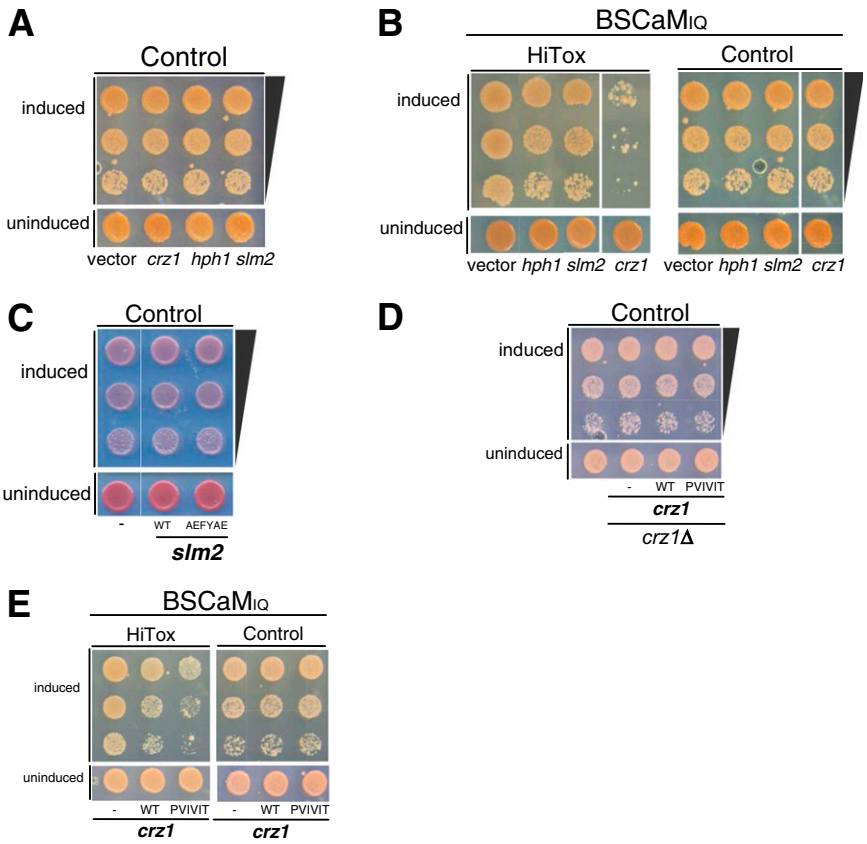

Fig. S6. Toxic and protective calcineurin substrates do not affect growth of the control yeast strain. (*A*) The control yeast strain was spotted onto plates containing uninducing media (SD −Leu; vector, *hph1*, *slm2* or *crz1* selective; *Lower*) and replica plated in threefold serial dilutions onto α-syn–inducing plates containing selective media and SGal −Leu (*Upper*). (*B*) Same assay as in *A* but in the presence of $BSCaM_{IQ}$. (*C*) The control strain was spotted onto plates containing uninducing media [SD −Leu; *slm2*, *AEFYAE-slm2* (unable to bind calcineurin) selective; *Lower*] and replica plated in threefold serial dilutions onto α-syn–inducing plates containing selective media and SGal −Leu (*Upper*). (*D*) The control strain was spotted onto plates containing uninducing media [SD −Leu; vector, *crz1*, *crz1*-PVIVIT (high affinity to calcineurin) selective; *Lower*] and replica plated in threefold serial dilutions onto α-syn–inducing plates containing selective media and SGal −Leu (*Upper*) in the presence and absence of *crz1* (*crz1*Δ). (*E*) The control and HiTox strains were spotted onto plates containing uninducing media [SD −Ura, $BSCaM_{IQ}$ selective, and SD −Leu; vector, *crz1*, *crz1*-PVIVIT (high affinity to calcineurin) selective; *Lower*] and replica plated in threefold serial dilutions onto α-syn–inducing plates containing selective media and SGal −Ura, Leu (*Upper*).

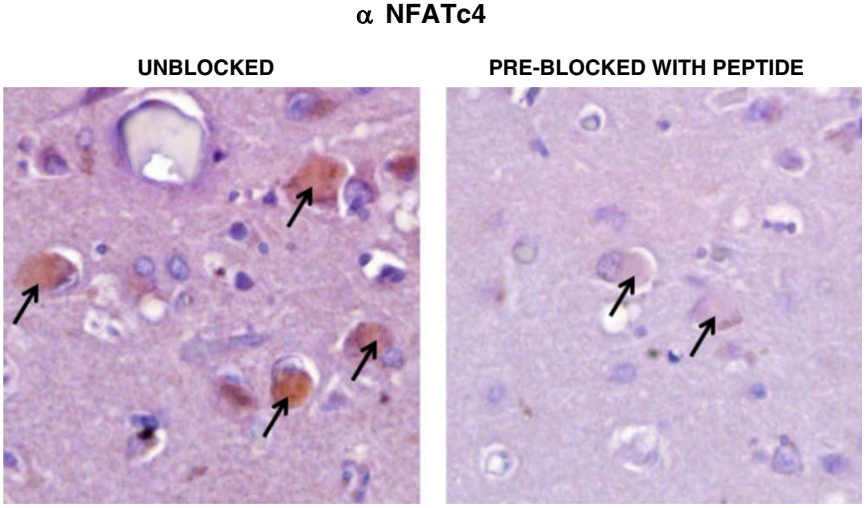

Fig. S7. NFATc4 staining is specific. (*Right*) Representative image from a human Parkinson disease (PD) cortex stained for NFATc4. (*Left*) Representative image of a similar area from the former individual preblocked with the peptide that was used to raise the antibody for NFATc4.

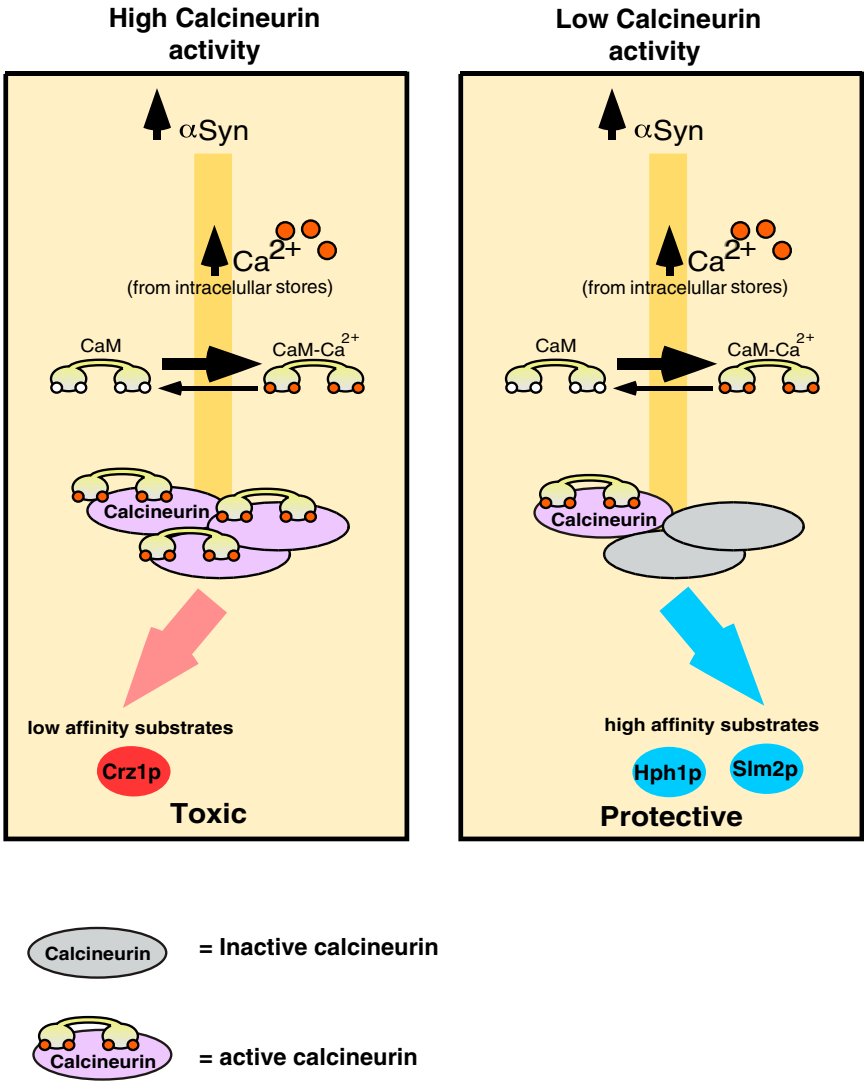

Fig. S8. Schematic of the proposed model. High levels of α-syn lead to a massive increase in cytosolic Ca^{2+} from intracellular stores, which bind to and activate calmodulin (CaM). High levels of CaM-Ca^{2+} lead to an overactivation of calcineurin molecules, which in turn dephosphorylate substrates such as Crz1p and/or other low-affinity susbtrates. This results in toxicity (*Left*). Alternatively, low doses of FK506, $BSCaM_{IQ}$, or low-affinity negative regulators such as Rcn2p, can reduce calcineurin activity and shift the balance to substrates like Hph1p and/or Slm2p (or presumably other high-affinity substrates) resulting in protection.